Emergence of a novel reassortant Oropouche virus drives persistent human outbreaks in the Brazilian Amazon region from 2022 to 2024

Felipe Gomes Naveca[1,2], Tatiana Amaral Pires de Almeida[1,3], Victor Souza[1], Valdinete Nascimento[1], Dejanane Silva[1], Fernanda Nascimento[1], Matilde Mejía[1], Yasmin Silva de Oliveira[1], Luisa Rocha[4], Natana Xavier[4], Janis Lopes[4], Rodrigo Maito[4], Cátia Meneses[4], Tatyana Amorim[5], Luciana Fé[5], Fernanda Sindeaux Camelo[5], Samyly Coutinho de Aguiar Silva[5], Alexsandro Xavier de Melo[5], Leíse Gomes Fernandes[5], Marco Aurélio Almeida de Oliveira[6], Ana Ruth Arcanjo[6], Guilherme Araújo[6], Walter André Júnior[6], Renata Lia Coragem de Carvalho[6], Rosiane Rodrigues[7], Stella Albuquerque[7], Cristiane Mattos[7], Ciciléia Silva[7], Aline Linhares[7], Taynã Rodrigues[8], Francy Mariscal[8], Márcia Andréa Morais[9], Mayra Marinho Presibella[10], Nelson Fernando Quallio Marques[10], Anne Paiva[11], Karina Ribeiro[11], Deusilene Vieira[12], Jackson Alves da Silva Queiroz[12], Ana Maísa Passos-Silva[12], Lígia Abdalla[13], João Hugo Santos[14], Regina Maria Pinto de Figueiredo[15], Ana Cecília Ribeiro Cruz[16], Livia Neves Casseb[16], Jannifer Oliveira Chiang[16], Livia Vinhal Frutuoso[17], Agata Rossi[18], Lucas Freitas[19], Túlio de Lima Campos[20], Gabriel Luz Wallau[20,21], Emerson Moreira[22], Roberto Dias Lins Neto[20], Laura W. Alexander[23], Yining Sun[24], Ana Maria Bispo de Filippis[2], Tiago Gräf[25], Ighor Arantes[2], Ana I. Bento[22], Edson Delatorre[18], Gonzalo Bello[2].

1. Núcleo de Vigilância de Vírus Emergentes, Reemergentes ou Negligenciados – ViVER/EDTA. Instituto Leônidas e Maria Deane, Fiocruz, Manaus, AM, Brazil;
2. Laboratório de Arbovírus e Vírus Hemorrágicos, Instituto Oswaldo Cruz, Fiocruz, Rio de Janeiro, RJ, Brazil;
3. Diretoria de Ensino e Pesquisa, Fundação Centro de Controle de Oncologia do Estado do Amazonas, FCecon, Manaus, AM, Brazil;
4. Laboratório Central de Saúde Pública de Roraima, Boa Vista, RR, Brazil;
5. Fundação de Vigilância em Saúde – Dra. Rosemary Costa Pinto, Manaus, AM, Brazil;
6. Laboratório Central de Saúde Pública do Amazonas, Manaus, AM, Brazil;
7. Laboratório Central de Saúde Pública de Rondônia, Porto Velho, RO, Brazil;
8. Laboratório Central de Saúde Pública do Acre, Rio Branco, AC, Brazil;
9. Núcleo de Doenças de Transmissão Vetorial, Secretaria Estadual de Saúde do Acre, Rio Branco, AC, Brazil;
10. Laboratório Central de Saúde Pública do Paraná, Curitiba, PR, Brazil;
11. Coordenação Geral de Laboratórios de Saúde Pública – CGLAB, Ministério da Saúde, Brasília, DF, Brazil;
12. Laboratório de Virologia Molecular, Fiocruz Rondônia, Porto Velho, RO, Brazil;

13. Universidade do Estado do Amazonas, Manaus, AM, Brazil;

14. Universidade Federal do Amazonas, Manaus, AM, Brazil;

15. Gerência de Virologia, Fundação de Medicina Tropical – Dr. Heitor Vieira Dourado, Manaus, AM, Brazil;

16. Department of Arbovirology and Hemorrhagic Fevers, Evandro Chagas Institute, Health and Environment Surveillance Secretariat, Ministry of Health, Ananindeua, PA, Brazil;

17. Coordenação-Geral de Vigilância de Arboviroses – CGARB , Departamento de Doenças Transmissíveis, Secretaria de Vigilância em Saúde e Ambiente, Ministério da Saúde, Brasília, DF, Brazil;

18. Laboratório de Genômica e Ecologia Viral, Departamento de Patologia, Centro de Ciências da Saúde, Universidade Federal do Espírito Santo, Vitória, ES, Brazil;

19. GISAID Global Data Science Initiative, Munich, Germany;

20. Instituto Aggeu Magalhães, Fiocruz, Recife, PE, Brazil;

21. Department of Arbovirology, Bernhard Nocht Institute for Tropical Medicine, WHO Collaborating Center for Arbovirus and Hemorrhagic Fever Reference and Research. National Reference Center for Tropical Infectious Diseases. Bernhard-Nocht-Straße 74, 20359 Hamburg - Germany.;

22. Universidade Federal de Pernambuco, Recife, PE, Brazil;

23. Department of Integrative Biology, University of California, Berkeley, CA, USA;

24. Department of Public and Ecosystem Health, College of Veterinary Medicine, Cornell University, Ithaca NY, USA;

25. Laboratório de Virologia Molecular, Instituto Carlos Chagas, Fiocruz, Curitiba, PR, Brazil.

ABSTRACT

The Brazilian western Amazon region is currently experiencing its largest laboratory confirmed Oropouche virus (OROV) outbreak, with nearly 6,000 reported cases in the states of Amazonas (AM), Acre (AC), Rondônia (RO), and Roraima (RR), between August 2022 and March 2024. Here, we sequenced and analyzed 382 full-length OROV genomes from human samples collected between 2022 and 2024 from all four states, aiming to trace the origin and genetic evolution of OROV leading to the current outbreak. Genomic analyses revealed that the recent upsurge of OROV cases in the Brazilian Amazon region coincides with the emergence of a novel reassortant viral lineage containing the M segment of viruses detected in the eastern Amazon region from 2009 to 2018 and the L and S segments of viruses detected in Peru, Colombia, and Ecuador from 2008 to 2021. The novel reassortant OROV lineage likely emerged in the Central region of the AM state between 2010 and 2014 and displayed a long-range silent dispersion during the second half of the 2010s. The 2022-2024 OROV epidemic was spatially segregated into three major subpopulations located in RR, AMACRO (a bordering region between AC, RO, and AM-Southern region), and AM-Central (which includes the Amazonas' capital, Manaus) regions. The peak of OROV transmissions in all regions occurred during the rainy season in the Amazon basin. Furthermore, our phylodynamics reconstructions showed that OROV spread was driven mainly by short-range (< 2 km) movements, with an average dispersal rate ≤ 1.2 km/day, consistent with the pattern of an active flight of infected vectors. Nevertheless, a substantial proportion (22%) of long-range (> 10 km) OROV migrations were also detected, consistent with viral dispersion via human activities. Our data provides an unprecedented view of the real-time spread and evolution of a neglected emergent human pathogen. Moreover, our results emphasize the need for widespread, long-term genomic surveillance to better understand the real burden of OROV within and beyond the Amazon region.

Main Text

Oropouche virus (OROV) is an arthropod-borne pathogen of the family *Peribunyaviridae,* genus *Orthobunyavirus,* species *Orthobunyavirus oropoucheense.* OROV is an endemic zoonotic arbovirus in the Amazon region that is maintained in a sylvatic transmission cycle among vertebrate hosts such as sloths, rodents, non-human primates, and birds by different vector species, including *Aedes serratus, Psorophora cingulata,* and *Haemagogus tropicalis*.[1,2] Similarly to the yellow fever virus (YFV), and in contrast to urban arboviruses such as dengue (DENV), Zika (ZIKV), and chikungunya (CHIKV), human infections are not essential to maintain the OROV life cycle. However, occasional OROV spillovers from wildlife to humans can initiate localized outbreaks or large epidemics once the virus is introduced to rural or urban settings[1]. OROV transmission in anthropogenic environments seems to be driven mainly by the biting midges *Culicoides paraensis*, although *Culex quinquefasciatus* mosquitoes have also been suggested as a possible secondary vector.[1,3–5] At least 30 human outbreaks of OROV have been irregularly reported in the Amazon region since the 1960s.[6]

Until the emergence of CHIKV and ZIKV in 2014-2015, OROV was the arbovirus with the second highest incidence in Brazil, only surpassed by DENV.[7] The country's largest documented OROV outbreak was reported in the Pará (PA) state in the late 1970s, where estimates based on serological, clinical, and epidemiology data pointed to >100,000 human cases [8]. During the 21st century, small outbreaks of OROV were documented in Manaus, the capital city of the Amazonas (AM) state in 2007-2008,[9] in a rural community of the Amapá (AP) state in 2008-2009[10], and in rural settings of the PA state in 2003-2004, 2006 and 2018.[11–13] However, the burden of OROV infections in Brazil has probably been underestimated due to the lack of systematic laboratory differential diagnosis and clinical symptoms similar to those of other endemic arboviral diseases.[14] Moreover, sporadic cases of OROV infection were detected between 2004 and 2016 in several municipalities of the AM, Acre (AC), Bahia, Mato Grosso, and Mato Grosso do Sul states with no reported outbreaks of this viral disease.[3,14–20] These data support a silent transmission and expansion of the OROV geographical boundaries within Brazil.

Between late 2022 and early 2024, the Brazilian states of AC, AM, Rondônia (RO), and Roraima (RR) located in the western Amazon region reported a sharp increase in the incidence of OROV cases.[21] As of 31st March 2024, 6,226 have tested positive for OROV (OROV+) by a real-

time RT-PCR protocol[22] in both rural areas and major urban centers of the western Amazon region (**Fig. 1a**). AM reported the highest number, with 3,685 notified cases, followed by RO (1,756), AC (441), and RR (344). This OROV epidemic is not only the most significant upsurge of human OROV cases in the 21st century but also the most geographically spread OROV epidemic ever documented, affecting over 140 municipalities from the Amazon basin (**Fig. 1a**), highlighting the risk of viral exportation and community transmission outside the Amazon basin. Since early 2024, dozens of autochthonous cases of OROV have been reported in non-Amazonian Brazilian states.[23,24] Thus, there is a crucial need to enhance our comprehension of the underlying mechanisms that fueled the current transmission of OROV in the Amazon region.

We then inspected the temporal pattern of OROV+ cases in the AM state, where extensive OROV testing occurred between November 2022 and March 2024 (**Fig S1a**). The data revealed that a very small first wave of OROV cases was recorded between late 2022 and early 2023, followed by a more significant second wave starting in October 2023, which dominated the epidemiological landscape of arboviral infections from December 2023 to March 2024 (**Fig. 1b**). The peak of OROV+ cases in the second wave coincides with the rainy season (from November to April) in the Amazon region (**Fig. 1c**), in line with previous OROV outbreaks/epidemics described in Brazil.[25] Rainfall after the dry season replenishes the soil with moist sites suitable for oviposition, immature development, and emergence of adult midges and coincides with higher levels of vector abundance.[26] Increased rainfall was associated with an expansion of the *C. paraensis* population in different settings of northern Brazil and in northwestern Argentina.[27] It was estimated that there would be a lag time of approximately 1-2 months between the initial increase in rainfall and the corresponding increase in the midge population in the Amazon biome.[28] These findings underscore the significant indirect effect of pluviosity on the increased transmission of OROV in the Amazon region, probably through its influence on the lifecycle of sylvatic/urban vectors.

The sylvatic nature of OROV transmission raises the hypothesis that potential vectors predominantly remain outside households, thereby increasing exposure risks for young, working-age males employed in forestry or other activities with frequent forest-dwelling animals/vector interaction. However, our results indicate that individuals from all age groups were infected with OROV (**Fig. 1c**). Additionally, the age distribution of infections was consistent across municipalities of varying sizes and degrees of urbanization (**Fig. 1d**). The adjustment of age

distributions to a Gaussian model indicated a slight skew towards older ages among individuals diagnosed with OROV (35.7 years, SD = 17.0) compared to those with DENV (32.3 years, SD = 17.9 years) (**Fig. S1b**) and sex distribution indicates a roughly equilibrium between sexes, with a male to female ratio of 1.09:1 in OROV cases, comparable to that observed in DENV cases (1.02:1, $P = 0.595$) (**Fig. S1c**). Interestingly, we detected co-infections of OROV with Mayaro virus (MAYV, n=1), with DENV type 1 (n=1) and with DENV type 2 (n=8) (**Fig S1d**). These findings suggest that the transmission of OROV follows a pattern like other urban arboviruses and highlights the need for integrated vector control strategies targeting both mosquitos and midges in urban environments of the Amazon region. Viral co-infections, albeit at low frequencies, also underscore the complex epidemiological landscape of arboviral infections and the potential interactions between different arboviruses during concurrent outbreaks in urban settings.

Fever (97.2%), headache (92.7%), and myalgia (78.2%) were the symptoms more frequently reported among the 2,272 OROV-positive patients from the AM state who answered the medical form in 2024. Other reported symptoms included nausea (42.1%), retro-orbital pain (34.1%), arthralgia (28.5%), vomiting (25.7%), photophobia (8.4%), diarrhea (7.4%), rash (2.8%), and edema (2.8%). Interestingly, two of these symptoms were more frequently observed in female patients: nausea ($P < 0.0001$) and vomiting ($P = 0.0005$) (**Supplementary Table 1**). So far, no fatal cases have been attributed to the disease. Clinical manifestations in the current outbreak were consistent with those observed in previous epidemics, where the most reported symptoms were fever (73-100%), headache (73-94%), myalgia (64-87%), and arthralgia (58-85%). These were followed by chills (10-64%), photophobia (17-58%), retroocular pain (14-65%), dizziness (10-42%), nausea (24-36%), vomiting (24%), diarrhea (10-13%), and rash (2-42%).[9,11–13,29–35] Of note, a significant proportion of patients (16%) infected in a previous OROV epidemic in Manaus in 2007-2008 had spontaneous hemorrhagic phenomena (petechiae, epistaxis, and gingival bleeding),[9] that were not observed in our study population. Thus, most OROV infections during the 2023-2024 epidemic in the AM state were mild and self-limited, with similar clinical manifestations to previous epidemics, as was recently described in the RO state.[36] These findings also support the notion that OROV diagnosis based solely on clinical symptoms is extremely difficult and reinforced the importance of implementation of accurate molecular diagnostic tests.[32]

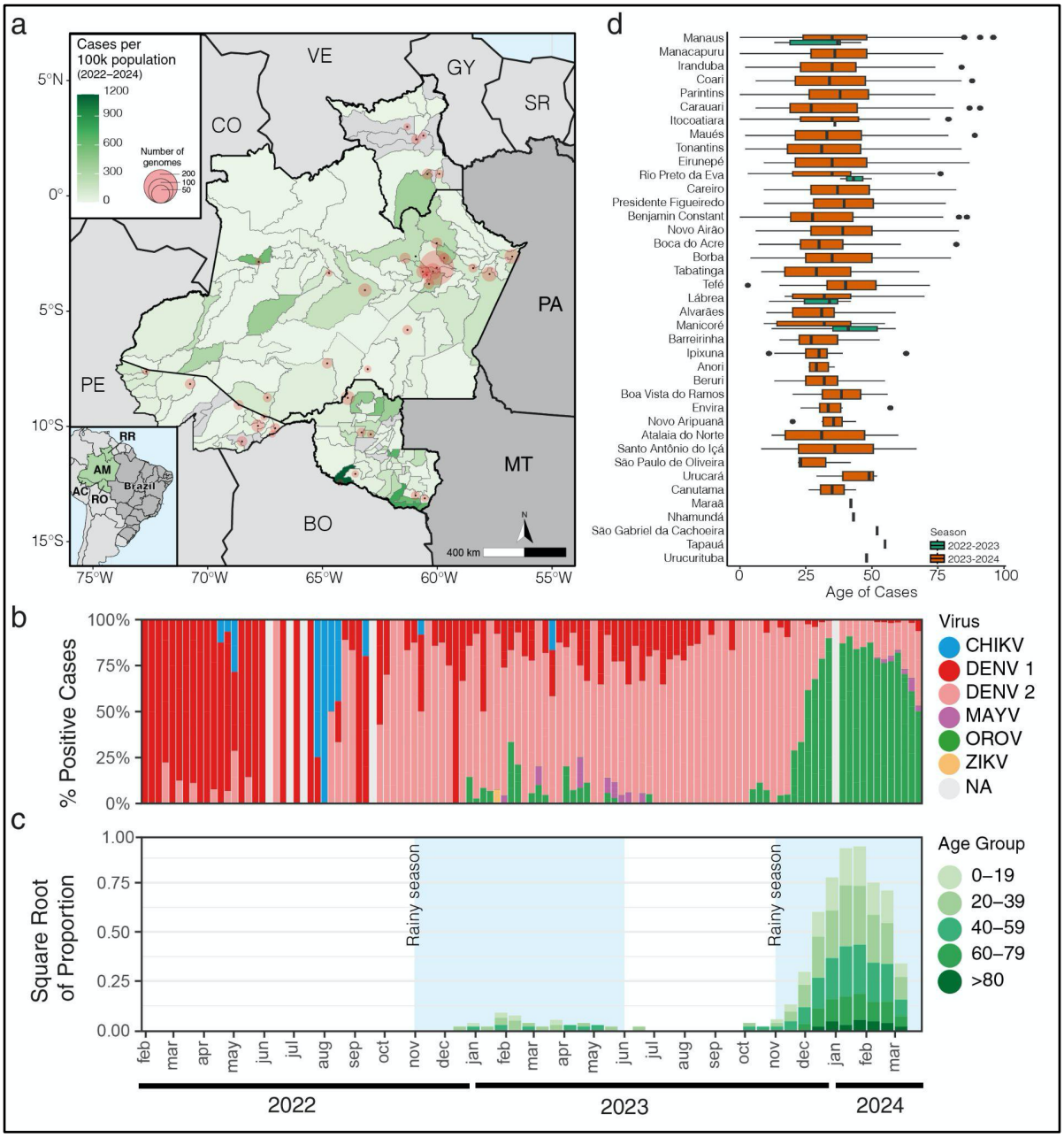

Figure 1. Epidemiological characteristics of the OROV outbreak in the western Amazonian Brazilian region (2022-2024). **a**) Geographic distribution of the OROV+ cases per 100,000 population diagnosed in Amazonas (AM), Acre (AC), Roraima (RR), and Rondônia (RO) between January 2022 and April 2024. Each municipality is colored based on the number of confirmed OROV-positive cases, as indicated by the color gradient in the top left legend. Additionally, circles represent the locations where OROV genomes were obtained, with circle sizes proportional to the number of genomes generated, as shown in the legend. The map also includes neighboring Brazilian states Pará (PA) and Mato Grosso (MT); as well as neighboring countries: Bolivia (BO), Peru (PE), Colombia (CO), Venezuela (VE), Guyana (GY), and Suriname (SR). **b**) Molecular positivity for arboviruses in the AM state, Brazil, from February 2022 to March 2024. **c**) Square root of the proportion of OROV-diagnosed cases biweekly, separated by age group. Blue-shaded areas indicate the Amazon basin region's rainy season (November through May). **d**) Box plot of the age distribution of OROV cases by municipality, illustrating the median and interquartile range (IQR) for the seasons 2022-2023 (green) and 2023-2024 (red).

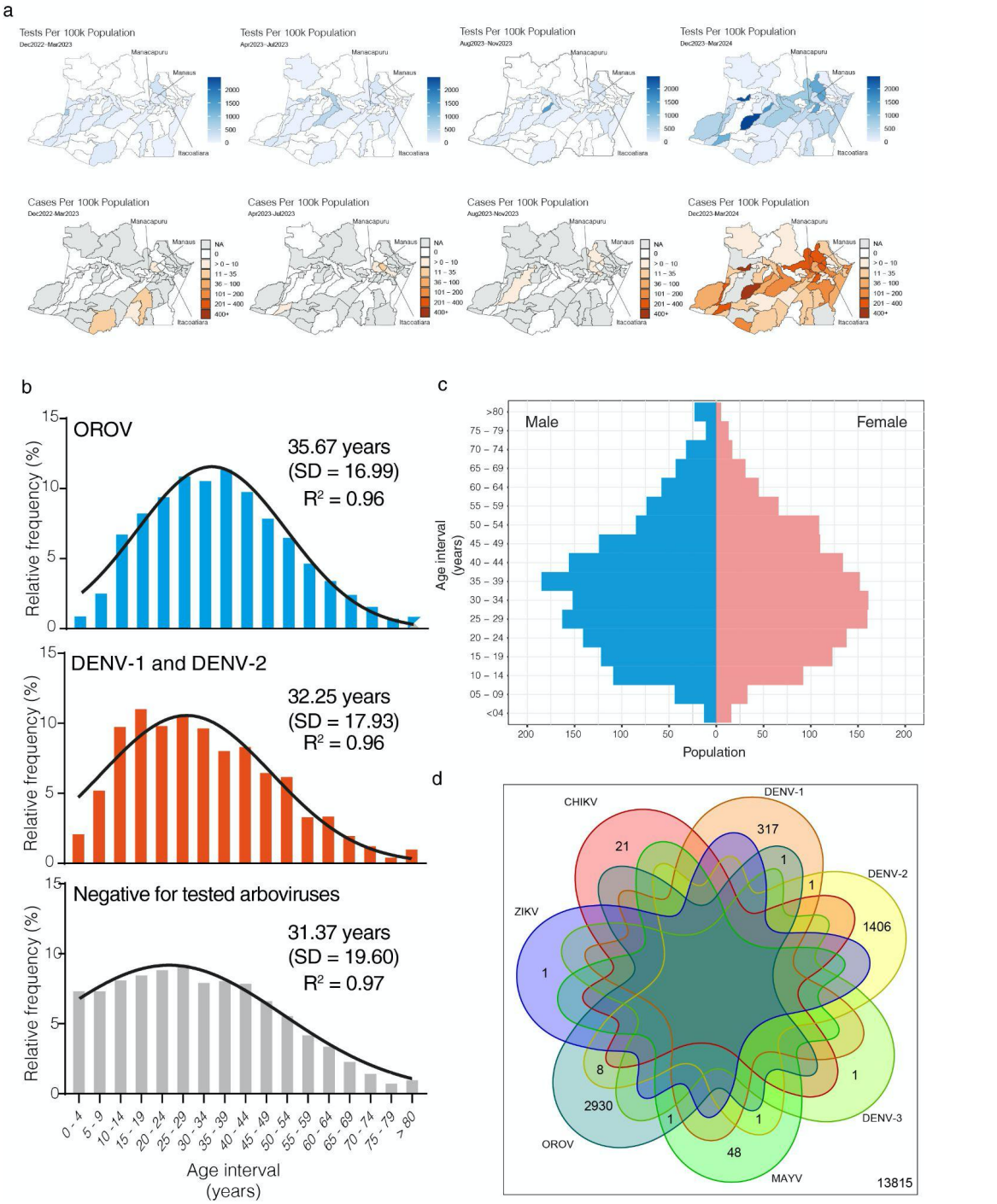

Figure S1. Comprehensive analysis of arboviral infections in the Amazonas (AM) state (2022-2024). a) Geographic distribution of RT-PCR tests for arboviruses (top panel) and OROV-positive cases per 100,000 population (bottom panel) in AM across four time periods: December 2022 to March 2023, April 2023 to July 2023, August 2023 to November 2023, and December 2023 to March 2024. Major cities (pop > 100k hab.) are indicated. B) Histograms depicting the age distribution of study patients in AM with different arboviral diagnosis profiles. Samples classified as ARBO-negative tested negative for OROV, Dengue virus (DENV), Zika virus (ZIKV), Chikungunya virus (CHIKV), and Mayaro virus (MAYV). C) Age-sex pyramid of the OROV-positive population from AM from 2022 to 2024, with males depicted on the left and females on the right. D) Venn diagram showing the distribution of detected viruses in the analyzed samples and the co-infections.

To understand whether the 2022-2024 west Amazon Brazilian OROV epidemic was fueled by one or multiple zoonotic events, and to estimate when and where the virus entered human populations and how the virus changed and spread as the current epidemic unfolds, we sequenced full-length OROV genomes from 382 patients living in 37 municipalities of the Brazilian states AM (n = 321), AC (n = 27), RO (n = 22), and RR (n = 12), collected between 30th August 2022 and 25th February 2024 (**Fig. 1a**). These 382 sequences were combined with all full-length OROV genome sequences available at the NCBI (n = 72), sampled in the Americas between 1955 and 2021, including the prototype sequences of OROV ($OROV_P$), Iquito virus ($IQTV_P$), Perdoes virus ($PEDV_P$), and Madre de Dios virus ($MDDV_P$). Bayesian phylogenetic analyses revealed two large well-supported ($PP \geq 0.90$) viral lineages for the M (M_1 and M_2) and L (L_1 and L_2) segments (**Fig. 2a-b**). The tree topology of the S segment was less resolved and sequences were dispersed across multiple clades (**Fig. 2c**), consistent with the notion that this segment contains less phylogenetic information than the segments M and L.[10,30,37] Using a minimum cut-off of clade size (n > 10 sequences) and support ($PP \geq 0.90$), we identified three major lineages (S_1, S_2, and S_3) and several minor lineages (S_X) for the S segment (**Fig. 2c**). These observations support the relevance of developing a phylogenetic classification system based on all the OROV gene segments as previously established for other segmented viruses such as rotavirus.[38] According to this system and the clades previously described, the $OROV_P$ prototype is classified as $M_1L_1S_1$, the $IQTV_P$ as $M_XL_2S_X$, the $PEDV_P$ as $M_XL_2S_3$, and the $MDDV_P$ as $M_XL_XS_X$.

The OROV sequences sampled in Brazil between 2022 and 2024 branched in a highly supported ($PP > 0.90$) monophyletic clade ($OROV_{BR\text{-}2015\text{-}2024}$) across all three genomic segments together with a sequence sampled in French Guiana in 2020 [31] and another sequence sampled in Tefé, AM, Brazil, in 2015 [14] (**Fig. 2a-c**). The OROV sequence from Tefé-2015 branched as the most basal strain of the $OROV_{BR\text{-}2015\text{-}2024}$ clade in all segments. The OROV sequence most closely related to the $OROV_{BR\text{-}2015\text{-}2024}$ clade differed between the M and the L+S segments. The $OROV_{BR\text{-}2015\text{-}2024}$ clade branched within the M_1 lineage, which comprises all OROV sequences sampled in Brazil since 1960 and was most closely related to a sister monophyletic clade ($OROV_{BR\text{-}2009\text{-}2018}$) that comprise sequences sampled in the eastern Amazonian states of AP in 2009 and PA in 2018 (**Fig. 2a**). In the L and S segments, the $OROV_{BR\text{-}2015\text{-}2024}$ clade branched within the L_2 and S_2 lineages, nested within a basal paraphyletic clade ($OROV_{PE/CO/EC\text{-}2008\text{-}2021}$) that encompass sequences sampled in Peru, Colombia, and Ecuador between 2008 and 2021 (**Figs. 2b-c**).

Interestingly, the $OROV_{BR\text{-}2009\text{-}2018}$ clade branched with high support with the $PEDV_P$ prototype in both L (L_2 lineage) and S (S_3 lineage) segments. Meanwhile, the $OROV_{PE/CO/EC\text{-}2008\text{-}2021}$ clade branched within the M_2 lineage, with sequences detected in Panama and Peru between 1989 and 2000 (**Fig. 2a-c**).

The considerable topological discordance among the phylogenetic trees of different genomic segments supports the occurrence of successive reassortment events throughout OROV evolution in South America, as schematically depicted in **Fig. 2d**. According to the proposed model, sequences sampled in Brazil between the 1960s and the 1990s mainly belong to the $M_1L_1S_1$ lineage. In contrast, sequences sampled in Peru between 1992 and 2000 belong to the $M_2L_2S_X$ lineage. The $OROV_{BR\text{-}2009\text{-}2018}$ clade detected on the eastern Amazon between 2009 and 2018[13,39] was probably a $M_1L_2S_3$ reassortant virus that possesses the M_1 segment from viruses already circulating in the Amazon region and the L_2+S_3 segments detected in the $PEDV_P$ isolated from a non-human primate (NHP) outside the Amazon basin in 2012.[13,39] The $OROV_{PE/CO/EC\text{-}2008\text{-}2021}$ clade detected in Peru, Colombia, and Ecuador from 2008 to 2021[37] was an $M_2L_2S_2$ virus that combined the M_2+L_2 segments of viruses circulating in Peru during the 1990s, along with a new S_2 segment that may have evolved from a basal S_X segment or may have been acquired from some unsampled OROV lineage. Finally, the $OROV_{BR\text{-}2015\text{-}2024}$ clade was a $M_1L_2S_2$ reassortant virus that acquired the M_1 segment from the $OROV_{BR\text{-}2009\text{-}2018}$ clade and the L_2+S_2 segments from the $OROV_{PE/CO/EC\text{-}2008\text{-}2021}$ clade. Reassortment is a powerful mechanism driving the evolution of bunyaviruses, and consistent with our findings, most recognized reassortants orthobunyaviruses possess L+S segments derived from one virus and M segment from another.[10,40–43] The balance between superinfection resistance, which promotes reassortments between distantly related viruses, and the compatibility of newly mixed components, which favors reassortments between closely related viruses, shapes productive exchanges.[43]

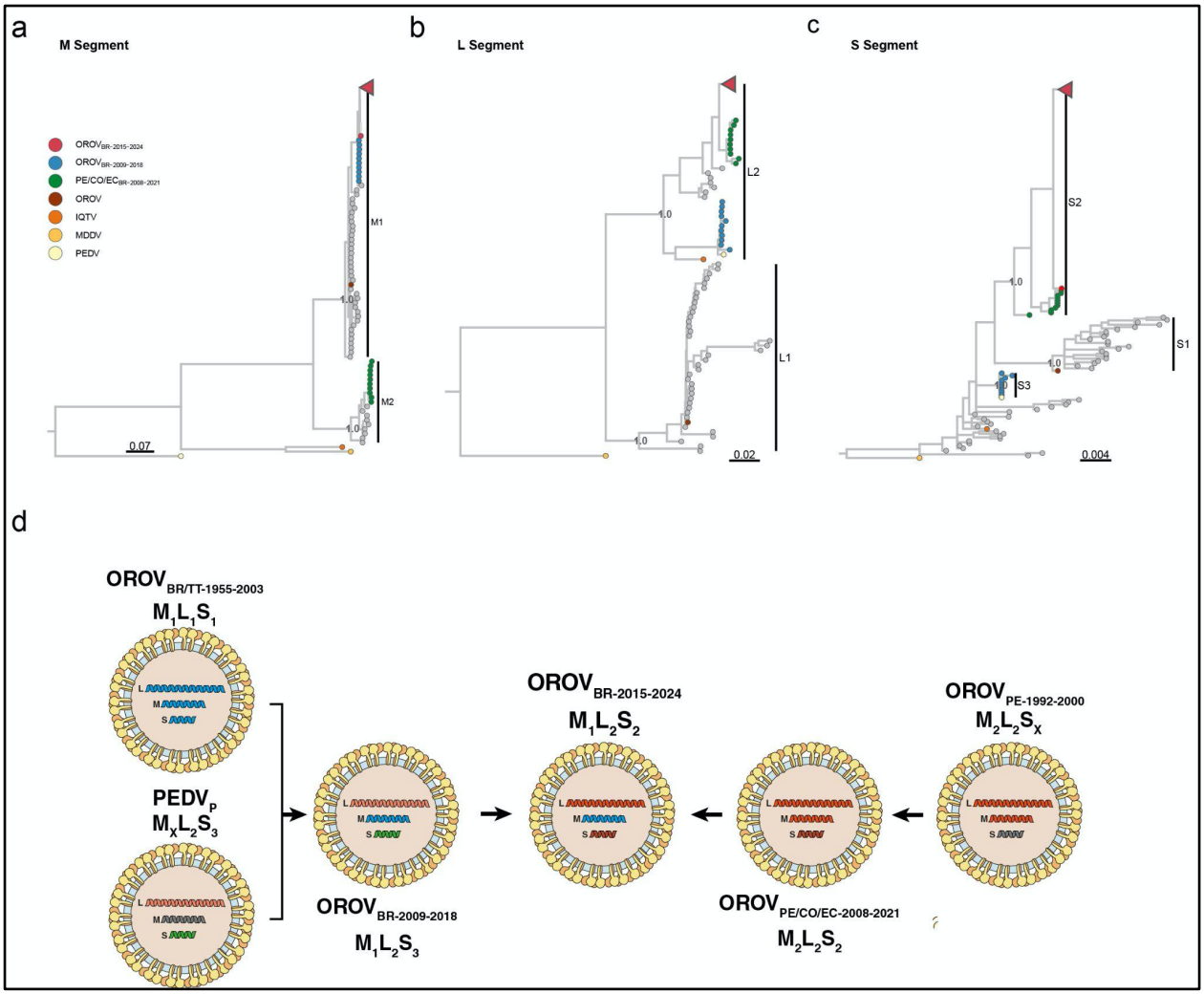

Figure 2. Phylogenetic analyses of the M, L, and S segments of OROV. a-c) Bayesian consensus tree inferred from the segments M (**a**), L (**b**), and S (**c**) of OROV sequences with complete genomes (n = 454). The tips of prototypical viruses and major clusters are color-coded according to the legend in the left corner. To improve visualization, the largest fraction of the $OROV_{BR2015-2024}$ was collapsed and indicated in the figure by a red triangle. Brackets demarcate major monophyletic lineages alongside their denomination and posterior statistical support. All trees are drawn according to the genetic distance scale at the bottom of each panel. d) Putative reassortment events that generated the current genomic diversity of OROV in South America. Each OROV genomic segment is colored according to the lineage identified in this study. Illustrations were obtained from SwissBioPics (https://viralzone.expasy.org/,[44]) and modified to align with the reassortment events hypothesis. OROV: Oropouche virus, IQTV: Iquitos virus, MDDV: Madre de Dios virus, PEDV: Perdões virus.

To track the time of the most recent common ancestor (T_{MRCA}) of the $OROV_{BR\text{-}2015\text{-}2024}$ clade and the time interval of the reassortment event, we reconstruct a Bayesian time-scale phylogenetic tree from the $OROV_{BR\text{-}2015\text{-}2024}$ clade plus their most closely related sequences belonging to the $OROV_{PE/CO/EC\text{-}2008\text{-}2021}$ clade in the L and S segments and the $OROV_{BR\text{-}2009\text{-}2018}$ clade in the M segment. The correlation between genetic divergence and sampling time was significant for datasets of all three genomic segments ($p < 0.05$). However, the temporal structure of the M segment (Correlation coefficient = 0.94) was more pronounced than that of the L and S segments (Correlation coefficient ~ 0.80) (**Fig. 3a-c**). The median estimated evolutionary rate for all three segments was roughly similar and ranged between 1.3 - 1.7 × 10^{-3} substitutions/site/year (**Fig. 3d**), although the shorter segment S presented higher estimates of uncertainty. Analyses of all three genomic segments traced back the median T_{MRCA} of the $OROV_{BR\text{-}2015\text{-}2024}$ clade to 2013-2014, slightly before the sampling time of the oldest sequence from that clade detected in Tefé-AM in 2015. The time frame of the reassortment event between clades $OROV_{BR\text{-}2009\text{-}2018}$ and $OROV_{PE/CO/EC\text{-}2008\text{-}2021}$ was estimated between 2009 and 2013 (**Fig. 3e-g**). OROV reassortment events were also reconstructed using the CoalRe model (**Figure S2**). Due to the considerably large genetic diversity of the virus and multiple reassortment events that likely took place in the OROV lineage's evolutionary history, MCMC for the CoalRe model only converged when a subsampled dataset of recent sequences (sampled from 2000 onward) was analyzed. The model estimated a reassortment rate of 0.1 [0.05 - 0.18, 95% highest posterior density (HPD)] events per year, which is very similar to what was previously estimated for p1918−like H1N1 and influenza B viruses.[45] However, the posterior probability (*PP*) of most of the reassortment events reconstructed by CoalRe was very low (*PP* <10), and only segment M reassortments showed intermediate to high support (purple dashed lines in **Figure S2**). The reassortment event that originated the $OROV_{BR\text{-}2015\text{-}2024}$ clade was highly supported (*PP* > 90) and probably occurred around 2010, in agreement with the pattern revealed by the independent analyses of the three viral segments. These findings support a short-term silent dispersion of the $OROV_{BR\text{-}2015\text{-}2024}$ clade during the first half of the 2010s before being detected for the first time in the small inner city of Tefé in the AM state in 2015 and subsequently in French Guiana in 2020.[14,31]

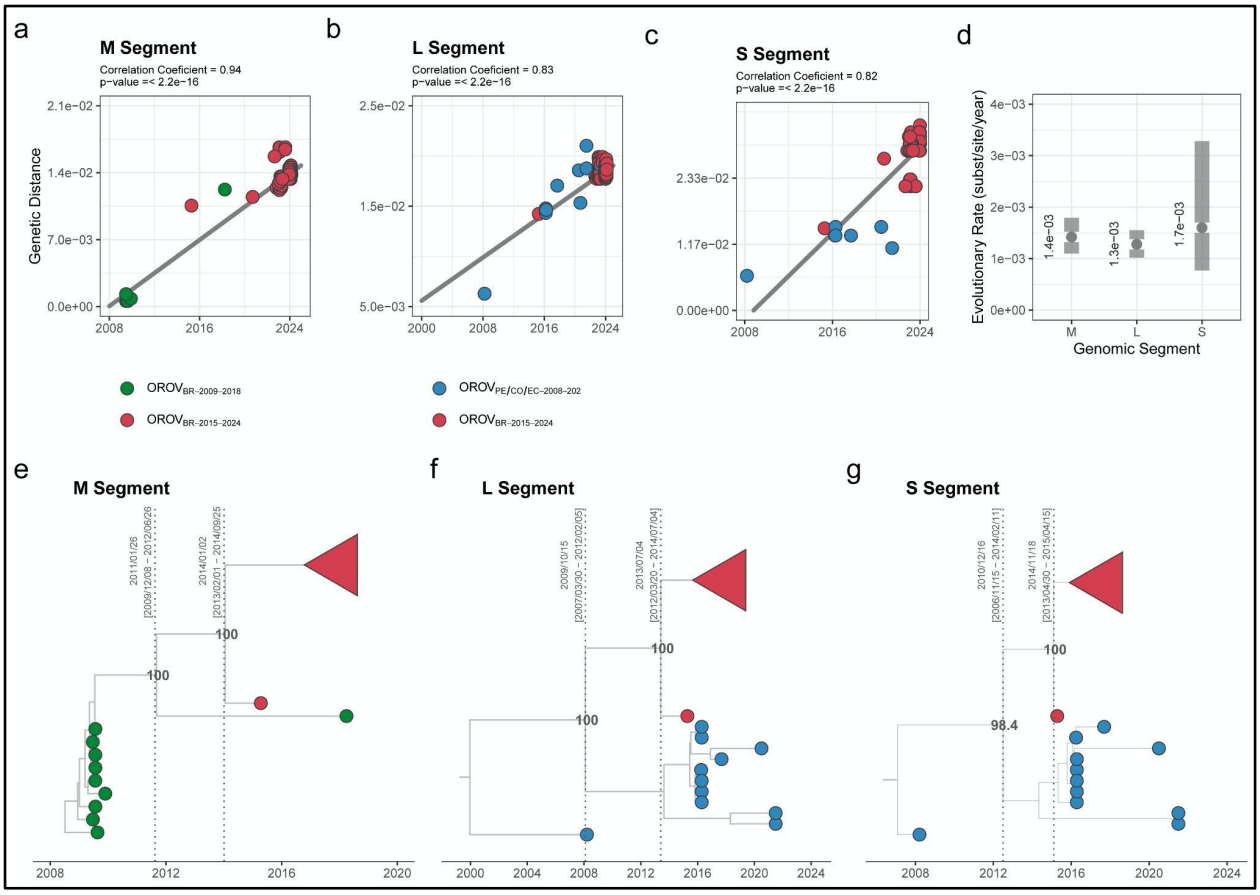

Figure 3. Temporal dynamics of the current outbreak OROV$_{BR\text{-}2015\text{-}2024}$ clade and the most closely related clades. The figure represents the root-to-tip linear regression between collection date and genetic distance (**a-c**), molecular clock median value and 95% HPD (**d**), and time-scaled Bayesian maximum clade credibility tree (MCCT) (**e-g**) inferred with datasets composed of the OROV$_{BR\text{-}2015\text{-}2024}$ clade (red tips) and its most closely related sequences of the OROV$_{BR\text{-}2009\text{-}2018}$ clade (green tips) in the M segment (n = 87) and of the OROV$_{PE/CO/EC\text{-}2008\text{-}2021}$ clade (blue tips) in the L (n = 88) and S (n = 88) segments. The posterior probability of key nodes in the MCCT are annotated. To improve visualization, the largest fraction of the OROV$_{BR\text{-}2015\text{-}2024}$ was collapsed in the MCCT in all three segments, as indicated by a red triangle.

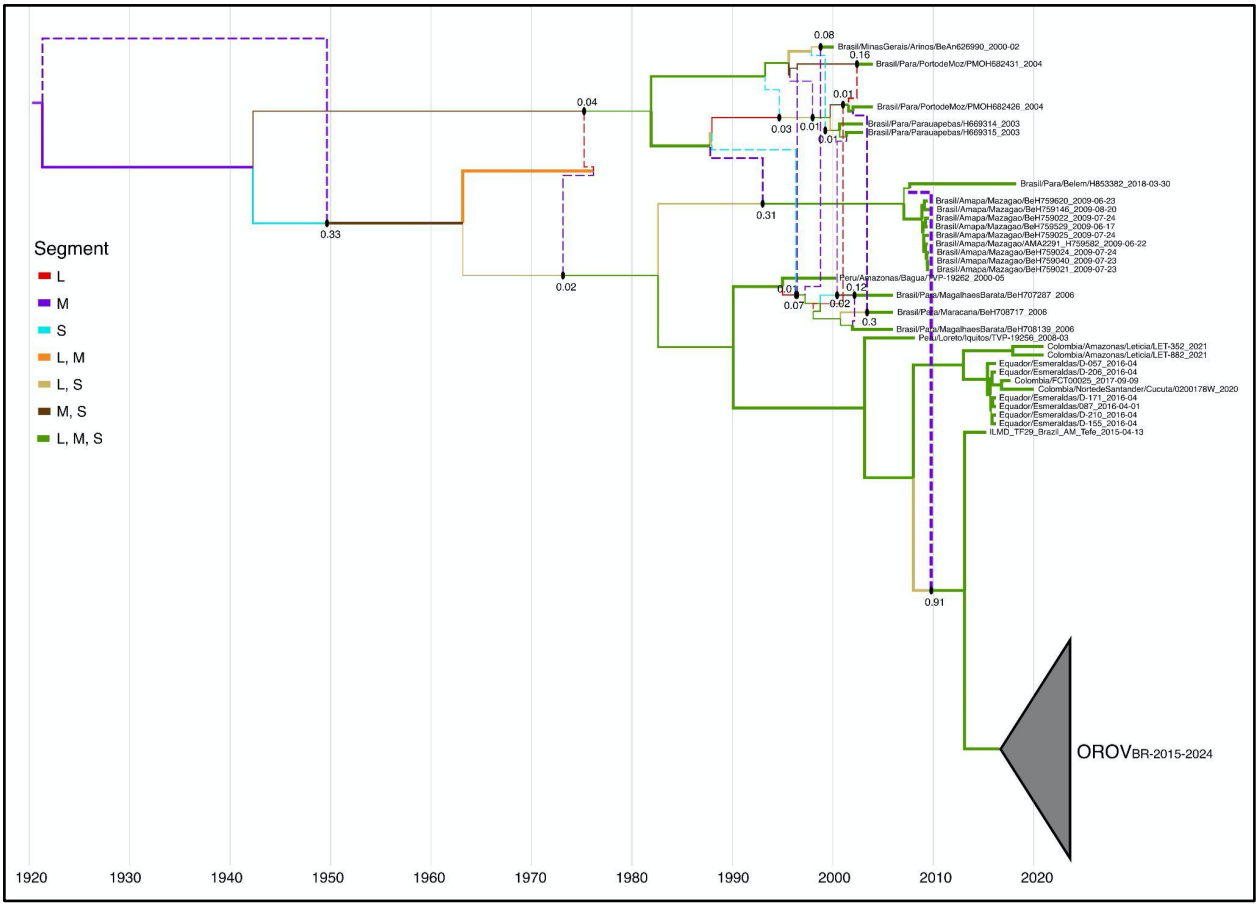

Figure S2. Maximum clade credibility (MCC) network of OROV complete genomes sampled after 2000. Reassortment events are represented as dashed-lines and the corresponding *PP* is shown. Branches thickness are according to the branch pp and colors represent the OROV segments carried by the branch as in the legend.

We used a Bayesian phylogeographic framework to reconstruct the spatial dissemination of the $OROV_{BR\text{-}2015\text{-}2024}$ clade in the Amazon basin, analyzing a concatenated full-length genomic dataset. The genome-wide molecular clock rate of the $OROV_{BR\text{-}2015\text{-}2024}$ clade was estimated at 1.2 $\times 10^{-3}$ (95% HPD: 1.1 - 1.4 $\times 10^{-3}$) substitutions/site/year. A discrete phylogeographic model was first employed to reconstruct the migration between states and regions in western Amazon: AC, RO, RR, Manaus, AM-Central, AM-South, AM-North, and AM-Southwest. Discrete phylogeographic reconstructions indicate that the $OROV_{BR\text{-}2015\text{-}2024}$ clade was spatially and temporally segregated in six major highly supported (*PP* > 0.90) lineages (**Fig. 4a-b**). The monophyletic sub-clade RR-I was exclusively composed of sequences from RR from August 2022 to May 2023. The paraphyletic sub-clade AMACRO-I was exclusively composed of sequences sampled in AMACRO, a bordering region of 454,000 km² between AC, RO, and AM Southern region (**Fig. 4c**) between December 2022 and May 2023. The monophyletic sub-clade AMACRO-II comprises all OROV sequences detected in AC, RO, and AM-South region from December 2023 onwards. OROV sequences detected in Manaus and AM-Central/Northern regions from November 2023 to February 2024 branched within the monophyletic sub-clades AM-I (83%), AM-II (11%) and AM-III (6%). The $OROV_{BR\text{-}2015\text{-}2024}$ clade was initially spread from the AM-Central region following two main routes (**Fig. 4a**). In the northward route, the virus reached RR (*PSP* = 1.0) around June 2022 and originated the RR-I sub-clade that drove multiple outbreaks in this state during the 2022-2023 rainy season, but we found no evidence of further dissemination beyond that period (**Fig. 4d**). In the southward route, the virus most probably first reached RO (*PSP* = 1.0) in August 2022 (**Fig. 4d**). However, this finding should be interpreted with caution due to uneven geographic sampling at late 2022, originating the AMACRO-I sub-clade. From RO, the AMACRO-I sub-clade rapidly spread to AC and AM-South, causing an epidemic wave in different municipalities of the AMACRO region during the 2022-2023 rainy season. This sub-clade persisted throughout the 2023 dry season and gave rise to four new sub-clades detected in the 2023-2024 rainy season: the AMACRO-II sub-clade most probably emerged in AC (*PSP* = 0.97) around August 2023 (**Fig. 4a-d**) and spread to RO and AM-South region, and the AM-I, AM-II and AM-III sub-clades that emerged in the city of Manaus (*PSP* > 0.95) between mid-August and early September 2023 (**Fig. 4a-d**). Subsequently, the AM-I and AM-II sub-clades spread from Manaus to other municipalities in the Central and Northern regions of AM state from December 2023 onwards (**Fig. S3**).

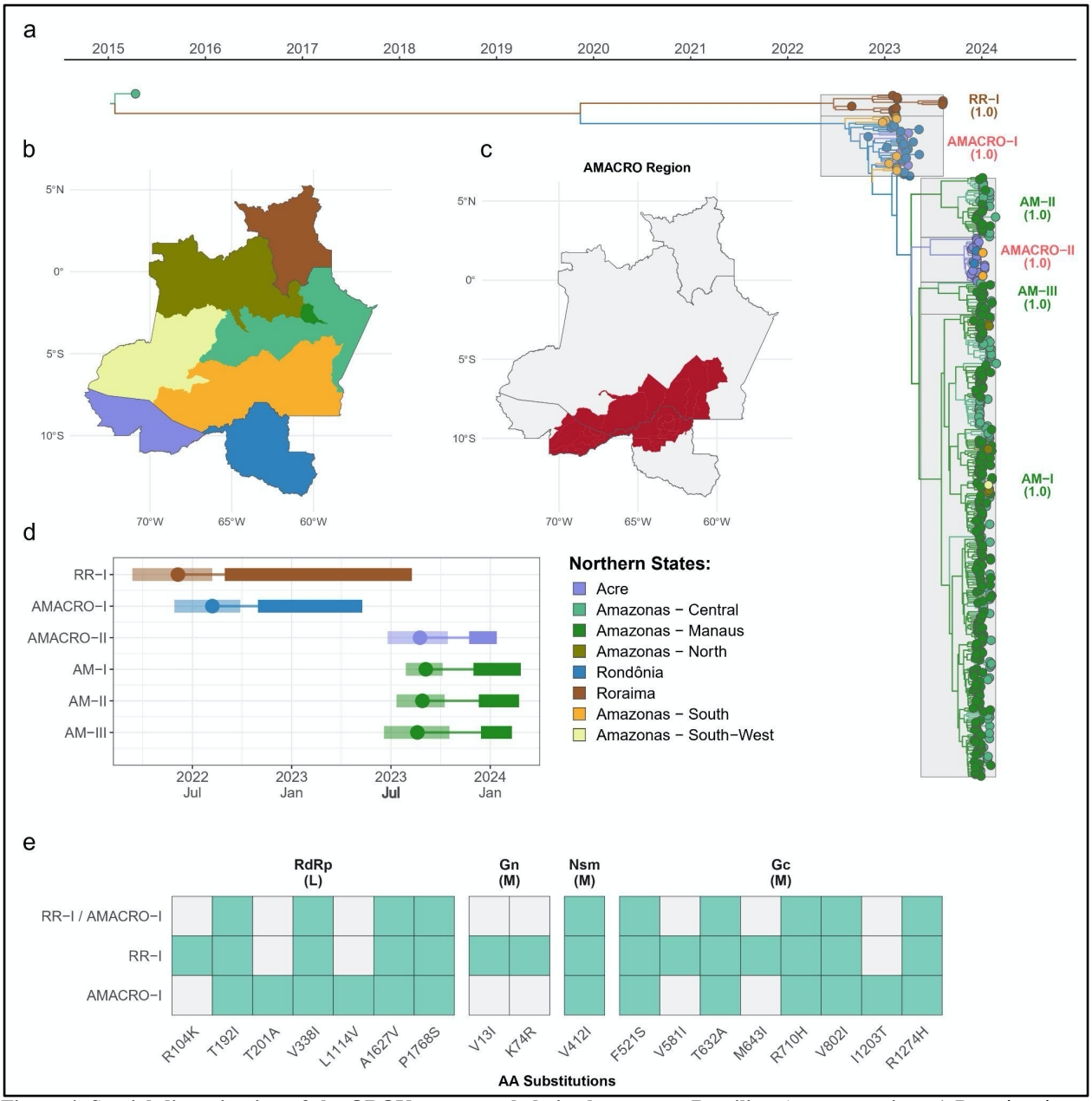

Figure 4. Spatial dissemination of the OROV$_{BR\text{-}2015\text{-}2024}$ clade in the western Brazilian Amazon region. a) Bayesian time-scaled MCC tree of the OROV$_{BR\text{-}2015\text{-}2024}$ clade, inferred after concatenation of the three genomic segments (L, M, and S) (n = 383). Branches are colored according to the inferred location of their ancestor nodes, and tips are colored according to sampling locations, both following the color scale shown in the bottom left corner of the tree. Sub-clades are highlighted in the tree alongside their posterior probabilities. **b-c**) Maps of the western Brazilian region, showing its constituent states, along with sub-state regions of Amazonas (**b**), both according to the same color scale used in the MCC tree and the supra-state AMACRO region (**c**). **d**) Temporal dynamics of major OROV$_{BR\text{-}2015\text{-}2024}$ sub-clades. For each sub-clade, we represent the time of the most recent common ancestor (T_{MRCA}, *circle*) and its 95% highest posterior density (HPD) interval (*transparent polygon*), the period of cryptic circulation (*thinner line*), and the sampling range (*thicker line*). Each sub-clade is colored following the same color scale used in the MCC tree. **e**) Amino Acid substitutions identified in the ancestral sequences of selected OROV clusters.

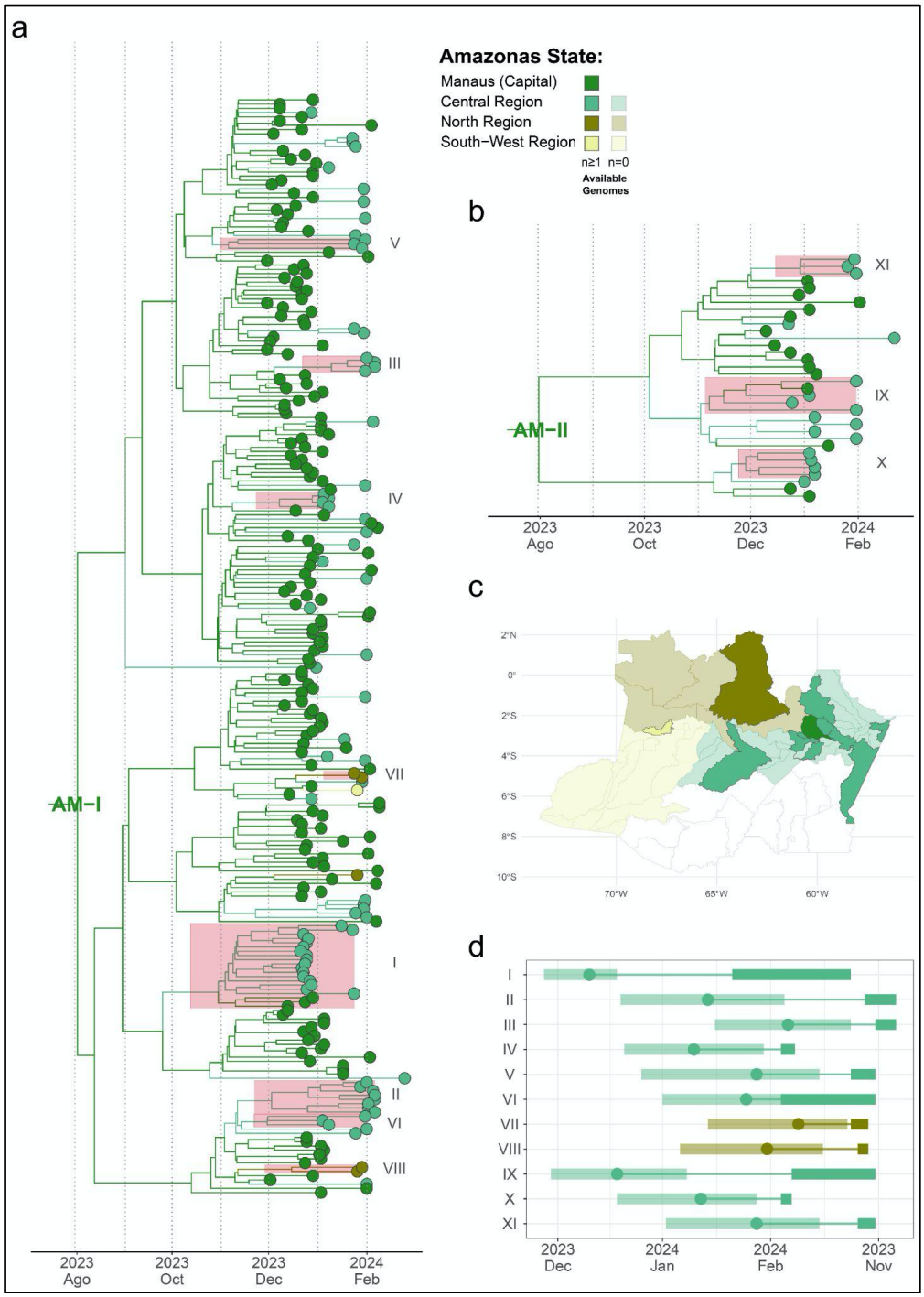

Figure S3. Spatial dissemination of the OROV$_{BR\text{-}2015\text{-}2024}$ clade in AM-Central/Northern regions a-b) Time-scaled MCC tree of the OROV$_{BR\text{-}2015\text{-}2024}$ AM-I (n = 259) (**a**) and AM-II (n = 34) (**b**) sub-clades, inferred after concatenation of the three genomic segments (L, M, and S) of each sample. Branches are colored according to the inferred location of their ancestor nodes, and tips are colored according to sampling locations, both following the color scale shown in the top right corner of the AM-I tree. Sub-clades are highlighted in the tree alongside their posterior probabilities. **c**) Map of Amazonas state, showing its sub-state regions, according to the same color scale used in the MCC tree. In each region, cities with available genomes are colored in a darker hue, as indicated in the legend. **d**) Temporal dynamics of major AM-I and AM-II sub-clades. For each sub-clade, we represent the time of the most recent common ancestor (T_{MRCA}, *circle*) and its 95% highest posterior density (HPD) interval (*transparent polygon*), the period of cryptic circulation (*thinner line*), and the sampling range (*thicker line*). Each sub-clade is colored following the same color scale used in the MCC tree.

The phylogeographic analysis revealed that OROV sub-clades detected in AC, RO and AM in 2024 evolved from a single common ancestor, suggesting that a small population of closely related viruses persisted in the AMACRO region throughout the 2023 dry seasons and fueled epidemics in the 2023-2024 rainy season. To confirm this hypothesis, we reconstructed the viral demographic dynamic using a BSKG model. This analysis supports an expansion of the *Ne* from November to March in the RR/AMACRO regions and a significant decrease between April and October, indicating a drastic viral population bottleneck following the transition from rainy to dry season (**Fig. S4**). In the AM-Central/Northern regions, the inferred *Ne* remained relatively stable from August to October and increased during the rainy season from November to February (**Fig. S4**). These findings support that the OROV epidemic in the western Amazon Brazilian region resulted from synchronous sub-epidemics occurring in RR and AMACRO (2022-2023 rainy season) and in AMACRO and AM-Central/Northern regions (2023-2024 rainy season). Viral movements within each subpopulation were frequent, whereas migrations between them were sporadic. The viral demographic pattern coincides with the seasonal pattern of OROV+ cases and was probably driven by alternating periods of high viral transmission during rainy seasons and low, but persistent, viral transmission during dry seasons.

Analysis of genomic variations in the $OROV_{BR\text{-}2015\text{-}2024}$ phylogeny reveals that several non-synonymous mutations were fixed across M (n = 11) and L (n = 7) genomic segments during recent evolution in the Amazon basin over the past decade (**Fig. 4e**), although most mutations fixed (90%) were synonymous. A total of 137 substitutions in the M (10 nonsynonymous and 47 synonymous), L (five nonsynonymous and 69 synonymous), and S (six synonymous) segments were detected at internal branches connecting the sequence sampled in Tefe-2015 with the MRCA of RR-I subclade, and 123 substitutions in the M (seven nonsynonymous and 34 synonymous), L (six nonsynonymous and 66 synonymous), and S (10 synonymous) segments at internal branches connecting Tefe-2015 with the MRCA of subclades circulating in AC, AM, and RO. Amino acid substitutions were mapped on glycoproteins, Gn (positions 1-300) and Gc (positions 482–1420), and the intervening NSm protein (positions 301-481) of the M segment. Interestingly, four substitutions occur in linear epitopes of Gn (8-28) and Gc (510-544, 616-632, and 706-718) glycoproteins recognized by the serum of immunized mice[46] and two others occur in linear B-cell epitopes of Gc (1197–1208) and NSm (409-416) proteins predicted by the use of bioinformatics tools.[47]

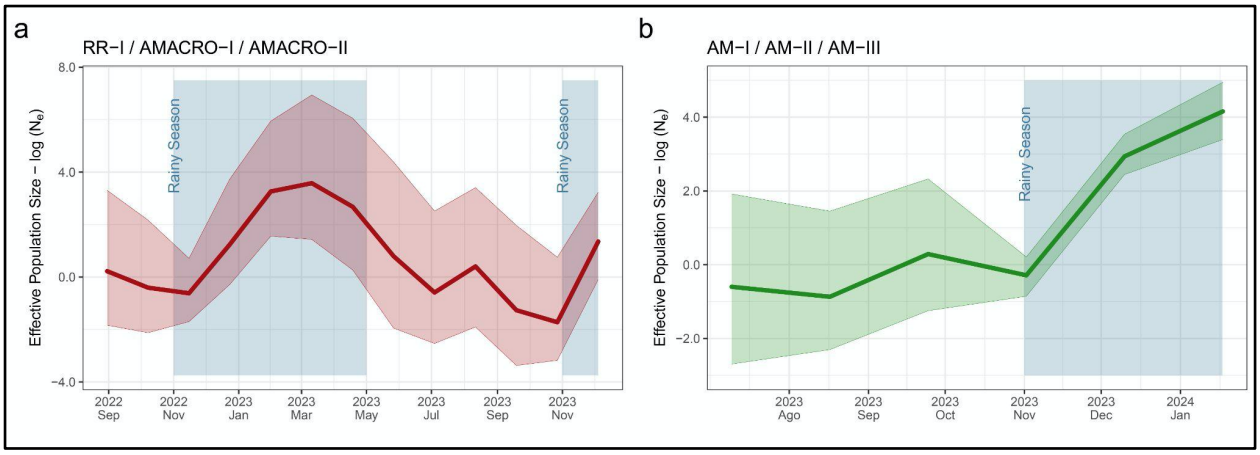

Figure S4. Demographic history of the main OROV$_{BR\text{-}2015\text{-}2024}$ sub-clades circulating in RR/AMACRO (a) and AM-Central/Northern (b) regions. Each plot details the effective number of OROV infections (*Ne*, y-axis) over time estimated under the coalescent-based Bayesian Skygrid (BSKG) model (posterior median = solid lines, 95% HPD = pale areas). Blue-shaded areas indicate the Amazon basin region's rainy season (November through May).

The geographical coordinates of the patient's residential area were employed to reconstruct the fine-scaled dispersion using a continuous spatial diffusion model with non-homogenous dispersion rates. The dispersion rate of viral lineages circulating in RR and AMACRO (RR-I+AMACRO-I+AMACRO-II) and those circulating in AM-Central (including Manaus) and AM-Northern regions (AM-I+AM-II+AM-III) were calculated separately (**Fig. 5a-b**). The average dispersion rate was estimated at 1.00 km/day (95% HPD: 0.79 - 1.26 km/day) in the RR/AMACRO regions and 0.66 km/day (95% HPD: 0.59 - 0.73 km/day) in the AM-Central/Northern regions, highlighting some differences in the OROV dynamics between these two areas (**Fig. 5c**). The viral dispersion rate also displayed some variation through time within each area (**Fig. 5d-e**). In the RR/AMACRO region, the viral dispersion rate remained stable at ~1 km/day (0.75 - 1.23 km/day) from August 2022 to March 2023, but it progressively increased from May 2023, reaching 1.65 km/day (1.21 - 2.14 km/day) by the end of December 2023. In the AM-Central/Northern regions, the viral dispersion rate decreased slightly from 0.74 km/day (0.67 - 0.81 km/day) in August 2023 to 0.65 km/day (0.59 - 0.72 km/day) in February 2024. Thus, during the 2023-2024 rainy season, the rate of viral dispersion in the AMACRO region was ~2.5x faster than in the AM-Central/Northern regions. Continuous phylogeographic reconstructions further revealed that very-short (<2 km), short (2–10 km), medium (11-30 km), and long (> 30 km) distance spread had a different impact on OROV dissemination, comprising 65%, 5%, 9% and 22% of all viral migrations, respectively (**Fig. 5f-g**).

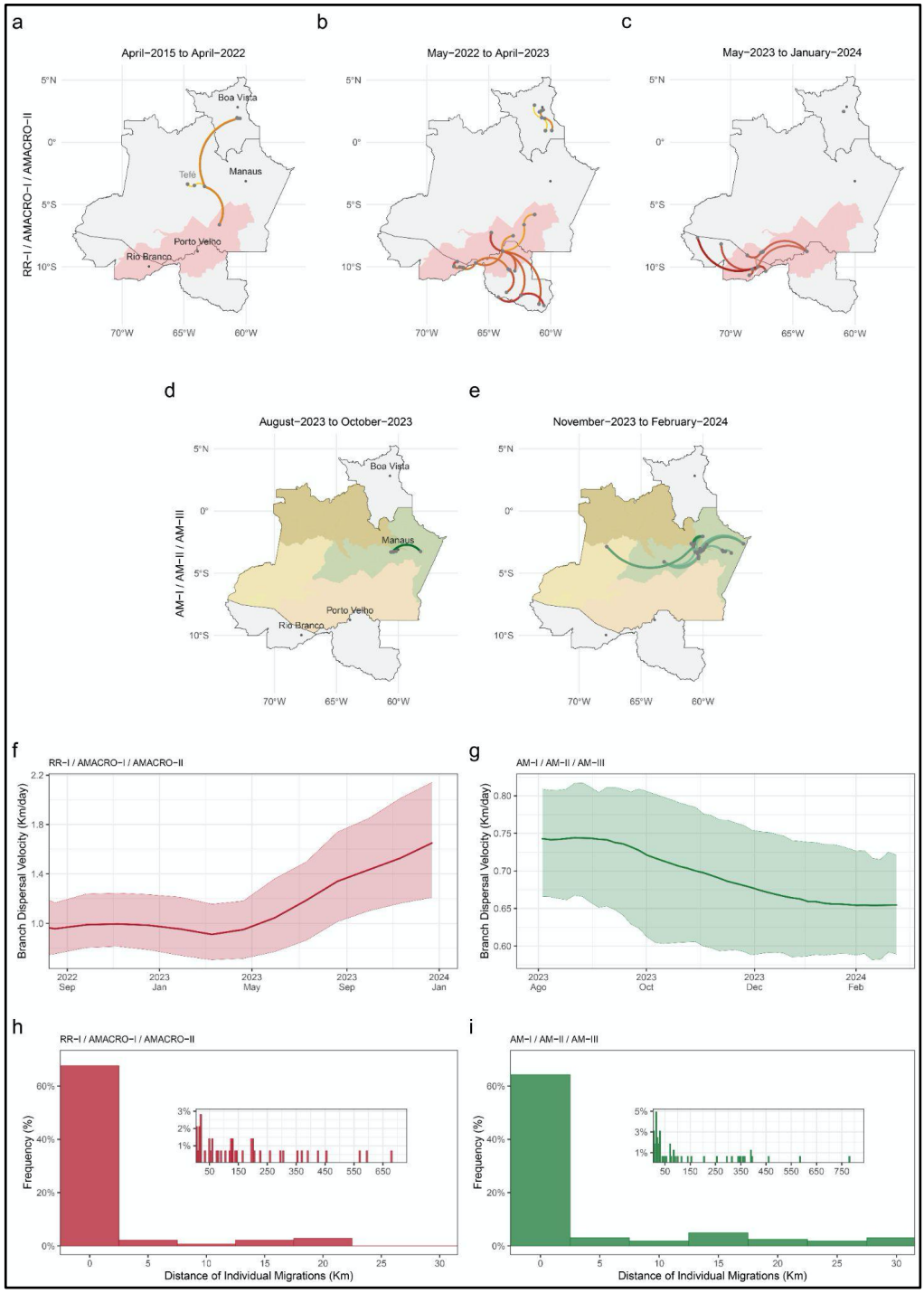

Figure 5. Spatiotemporal dispersal of the main OROV$_{BR\text{-}2015\text{-}2024}$ sub-clades circulating in RR/AMACRO and AM-Central/Northern regions estimated from the continuous diffusion phylogeography process. a-b) Lines represent MCC tree branches of the RR/AMACRO (**a-c**) and AM central and northern regions subclades (**d-e**) projected on the maps according to the location of internal phylogenetic nodes and tips. Lines are shaded in gradients that transition from lighter to darker hues, representing the passage of time within each panel and connecting the origin and destination of migrations using a clockwise curvature. Major cities are annotated in the first panel of each sequence. **f-g)** OROV epidemic weighted branch dispersal velocity through time (posterior median = solid lines, 95% HPD = pale areas). **h-i)** Histograms of the frequency distribution of short (< 5km), medium (5 – 30 km), and long (> 30 km) distance viral migrations calculated from the branches of 1,000 randomly selected trees from the posterior distribution of the continuous phylogeographic analysis.

The pattern of OROV spread in the Amazon region, characterized by short-range (< 2 km) movements along continuous and contiguous areas with an average dispersal rate of ≤ 1 km/day, is entirely consistent with the pattern of active flight during the lifespan of infected vectors. Sylvatic mosquitoes in Brazil may move up to 3 km/day,[48] and *Culicoides* spp. in North America display a mean dispersal rate of ~2 km/day and typically travel <5 km from their breeding sites.[26,49,50] Interestingly, the mean rate of spatial dispersal of OROV in the Amazon region is roughly similar to the spread rate of sylvatic transmission estimated for the YFV in the Americas (0.50 km/day)[51] and Brazil (0.50-1.42 km/day).[52–54] These findings suggest that the dispersal of infected vectors was probably a major driving force of the spatial spread of OROV in the Amazon basin. A significant proportion (31%) of OROV migrations, however, traveled medium and long distances (> 10 km) consistent with viral dispersion via infected humans. It is presumed that some individuals acquire the infection in the forest and later visit a rural or urban setting during the viremic phase, acting as a source of infection for biting midges and as the probable link between the sylvatic and urban transmission cycles of OROV.[1] This potential link between sylvatic and urban transmission cycles of OROV adds a layer of complexity to disease control strategies. The expansion of transportation networks in the Amazon region also significantly increases human mobility and rapidly connects forest regions and rural settlements with urban areas, and may thus foster the spread of zoonotic infections among humans.[55] The movement of infected individuals by terrestrial and air travel could have mainly contributed to the spread of OROV between non-contiguous rural and urban areas, rapidly expanding the geographic boundaries of viral transmission within the Amazon region and beyond.

While annual variations in rainfall may contribute to the seasonality of OROV transmission observed between 2023 and 2024, this factor does not explain the inter-annual variability in OROV epidemics nor the singular characteristics of the current OROV epidemic in the Amazon basin, which is distinguished from the previous ones by the longer duration and broader geographic extension. While previous outbreaks/epidemics generally last a single rainy season and impact one urban area or a few inner cities of a given state, the current epidemic spans at least two consecutive rainy seasons. The current outbreak affects over 140 municipalities across four northern Brazilian states, encompassing an area of approximately 2 million km^2. Some additional key factors that operate on different timescales might have combined to alter the ecological dynamics of OROV in recent years, increasing the risk of zoonotic spillovers and the subsequent amplification of viral

transmissions among humans in the Brazilian Amazon region. Viral evolution, anthropogenic landscape perturbations, and global climate changes are critical drivers of oscillations in the incidence and geographic spread of arboviral diseases in human populations.[56]

OROV evolution can occur in very short timescales due to the high mutation rate and the capacity of genetic reassortment, allowing the virus to acquire key adaptive mutations rapidly.[57] We hypothesize that the upsurge of OROV cases in western Amazon was driven by the emergence of a novel reassortant clade $OROV_{BR\text{-}2015\text{-}2024}$ with enhanced viral transmissibility in sylvatic and/or urban cycles. However, the clade $OROV_{BR\text{-}2015\text{-}2024}$ circulates endemically in the Amazon basin for almost a decade without causing large outbreaks.[31] It could be argued that clade $OROV_{BR\text{-}2015\text{-}2024}$ accumulated key mutations since 2020 that potentially increased viral transmissibility. However, the lack of similar large OROV epidemics in the eastern Brazilian Amazon region (PA and AP states) does not support this hypothesis. Further studies are essential to compare the replicative and infective potential between past and current circulating OROV lineages and to test if some mutations fixed during the recent evolution of OROV may impact virological traits such as infectivity or immune evasion. Without these data, we cannot rule out that additional factors beyond viral evolution drive the explosive OROV epidemics in the western Amazon between 2022 and 2024.

Extreme environmental changes may influence the long-term transmission dynamics of arboviruses,[58–61] and current OROV outbreaks in the Amazon region coincide with remarkable El Niño Southern Oscillation (ENSO) events and extreme climatic events. The period of silent dissemination of the novel OROV reassortant strain (2011-2021) coincides with a high frequency of severe floods in the Amazon basin.[62–64] The current OROV epidemic, from November 2022 to March 2024, was foregone by unprecedented flooding events in the southwestern Amazon region during 2020-2021 caused by a rare multi-year 2020-23 La-Niña event.[65,66] Moreover, the current OROV epidemic overlapped with the transition from the 2022-23 La Niña to the 2023-24 El Niño, which caused record drought and heat in the Amazon basin.[67] Southwestern Amazonia experienced negative rainfall anomalies from November 2022 to February 2023, while northern Amazonia faced damaging rainfall and record-high temperatures from June to September 2023. Climatic extremes have become more widespread and frequent across Amazon[68], which may have changed the OROV endemic and epidemic transmission dynamics.

Fragmented forest landscapes and vegetation loss due to deforestation and expanding agricultural land use were pointed as key drivers of OROV transmission.[69–71] Alarming growing deforestation trends have been observed in the Brazilian Amazon region since 2018, mainly driven by illegal land grabbing, timber extraction, mining, and agricultural expansion into forested lands.[72] Most OROV-positive localities in 2022-2023 were concentrated in AMACRO, an area considered the new frontier of deforestation that was responsible for a significant fraction of forest lost in the AM (82%), RO (77%), and AC (63%) states between 2017 and 2021.[72–74] Similarly, critical deforestation areas in the RR state were close to the municipalities of Alto Alegre, Mucajaí, Iracema, and Rorainópolis,[72] which concentrated most OROV-positive cases in the state. The weakening of environmental governance in Brazil between 2018 and 2022 certainly acted as a stimulus for the advance in deforestation across all Amazonian regions.[75–78] The accelerated deforestation in the AMACRO region further coincided with its designation as a special zone for agricultural development,[79–81] the expansion of agribusiness activities reliant on expanding frontiers by clearcutting forests,[79,82] and the improvement of the infrastructure like the highway BR-319, which connect the state capitals of AM and RO and crosses several conservation units and Indigenous lands.[75,83–86]

Although establishing direct causality between events is challenging, the circumstantial evidence described above points to a putative link between current OROV outbreaks and extrinsic environmental factors that culminate in higher pathogen exposure to the human population in Brazilian Amazon.[87] Synergistic interactions between uncontrolled deforestation, agricultural encroachment, road construction, extreme flows, and warming droughts over the last few years may have altered the ecological conditions for endemic/urban OROV transmission and further increased the number of susceptible people near new forest edges in the western Brazilian Amazon. These factors combined increase the risk of viral spillovers from wildlife to humans and the subsequent human-to-human transmissions within rural and urban settings of the Amazon region. The absence of similar OROV outbreaks at deforestation frontiers in the eastern Amazon (AP and PA states) might be explained by intrinsic factors such as a lower abundance of susceptible hosts. Due to the longer history of forest degradation and OROV outbreaks, people from the eastern Amazon could have been more frequently exposed to the virus, making them less susceptible to infection than people from neo-colonized areas in the western Amazon.

Our study has some limitations. First, the 7-year gap between the earliest sampled OROV sequence of the current outbreak and the most closely related non-outbreak sequence sampled in Tefe in 2015 limits our ability to reconstruct the pattern of viral spread pre-2022 accurately. Second, geographic-based sampling bias during the current outbreak may have affected the accuracy of phylogeographic reconstructions. Hence, many apparent long-distance viral migrations may have resulted from sequential shorter-range migrations between unsampled locations.[88–90] Despite this potential limitation, phylogeographic inferences performed using different datasets (complete or downsampled) and methods (discrete or continuous) recovered similar spatiotemporal patterns. Third, the absence of long-term laboratory surveillance of OROV cases in Brazil hinders our ability to determine whether recent upsurges are due to enhanced surveillance efforts or to enhanced viral transmission. Finally, we have no information about the primary vector involved nor about temporal changes in vector abundance and biodiversity across sylvatic, forest edges and urban environments in more affected areas during the ongoing 2022-2024 OROV outbreak.

In summary, our findings revealed that a new reassortant OROV lineage that circulated in the Amazon region for about one decade caused an upsurge of OROV cases in several rural and urban settings of the western Amazon Brazilian region between 2022 and 2024. Our results confirm the high epidemic potential of OROV in the Amazonian biome and raise concerns about the risk of spreading and establishing this neglected arbovirus outside the Amazon region. Indeed, recent findings support that the $OROV_{BR\text{-}2022\text{-}2024}$ clade was successfully established in the Southeastern and Southern Brazilian regions and the Caribbean region by early 2024.[21] Our study also warns about the crucial need for the widespread distribution of diagnostic tests for the detection of OROV across all Brazilian states. Further studies will be needed to assess whether the recent evolution of OROV might have changed vector competence and virus transmissibility in wild or urban cycles. Moreover, the implementation of long-term interdisciplinary "One Health" disease surveillance systems is needed to understand the relationship between extrinsic environmental factors, wildlife biodiversity, and the dynamics of OROV infections in human and wild reservoir hosts. Such information is crucial to identify “pathogenic landscapes” that may increase the risk of OROV transmission[91] and to develop early warning systems for OROV epidemics.

METHODS

OROV positive samples and ethical aspects. Acute OROV infection was detected using a duplex reverse-transcription real-time PCR assay previously developed by our team in Manaus that simultaneously detects OROV and Mayaro viruses.[22] This protocol was recently implemented in all Central Public Health Laboratories located in each Brazilian State (LACEN) by the Brazilian Ministry of Health and was also recommended by the Pan-American Health Organization for the molecular diagnosis of OROV and Mayaro viruses (https://www.paho.org/en/documents/real-time-rt-pcr-protocol-mayaro-mayv-and-oropouche-virus-orov-duplex). The Central Laboratories from the States of AM (LACEN-AM), RR (LACEN-RR), RO (LACEN-RO), and AC (LACEN-AC), as well as Fiocruz Rondônia, sent OROV positive samples for sequencing at Instituto Leônidas e Maria Deane (ILMD - FIOCRUZ Amazônia), that is the hub of FIOCRUZ Genomics Surveillance Network of the Brazilian Ministry of Health in Manaus, AM for viral genome characterization. Information regarding the week and location of the collected samples analyzed in this study and their phylogenetic context (considering the M segment) may be visualized in detail on our Microreact [39] page: https://microreact.org/project/orov-north-2022-2024. This study was approved by the Ethics Committee of Amazonas State University (CAAE: 72678923.8.0000.5016), which waived signed informed consent.

Epidemiological data. Individual-level data: case line-list data was retrieved from GAL (Gerenciador de Ambiente Laboratorial) at the municipality level for the states of Acre, Amazonas, Roraima, and Rondônia between January 2022 and March 2024. For Amazonas, all arboviral notifications for the period were recorded. Each case had a notification code and metadata associated with it which included demographic characteristics, spatial location, laboratory results and clinical details such as symptoms, hospitalization status, and dates associated with notification, and onset with these were reported at least for most cases. For the other states, only the information about OROV detection was retrieved. Identifiers were anonymized. Data Cleaning: We identified and merged any duplicate entries in the line-list. And reconciled dates where onset date was in discrepancy with notification date. Demographic data. Demographic data for ages at the level of municipality from the 2022 census was retrieved from the Brazilian Institute of Geography and Statistics (https://sidra.ibge.gov.br/pesquisa/censo-demografico/demografico-2022/universo-populacao-por-idade-e-sexo). These data were used to calculate age specific incidence of reported OROV cases. Medical records: An investigation of the clinical symptoms was conducted by the

Amazonas State Health Surveillance Foundation - Dr Rosemary Costa Pinto (FVS-RCP) among the 2,272 OROV-positive patients from the AM state who answered the medical form in 2024.

OROV amplification and sequencing. We sequence one full-length OROV genome (Tefé-2015) using an unbiased metatranscriptomics protocol (Illumina Ribo-ZeroTM Plus Microbiome Depletion Kit). This comprehensive sequencing, along with other complete genomes available in GenBank, served as a pivotal reference for the design of an amplicon-based strategy using Primal Scheme [92] and a modified version of Primer3 [93] embedded in Geneious Prime 2023.2.1 (**Supplementary Table 2**). All other OROV genome amplification and sequencing libraries were prepared with Illumina COVIDSeq backbone for a more cost-effective genome-wide sequencing strategy. However, with our newly OROV-designed primers on 2 × 150 cycles paired-end runs. Raw sequencing data was collected with MiSeq Control Software v2.6.2.1 or NextSeq 1000 Control Software Suite v1.2.0. Subsequently, it was converted to FASTQ files on Illumina's cloud-based application (https://basespace.illumina.com). FASTQ files were imported to Geneious Prime v2023.2.1, trimmed, and assembled into contigs using a workflow customized by our group employing BBDuk, Dedupe, and BBMap tools (v.38.84), embedded in Geneious Prime. The GenBank sequences OL689332, OL689333, and OL689334 were used as templates for the S, M, and L Oropouche virus segments. All contigs were visually inspected before consensus calling using a threshold of at least 50%. Finally, using this sequencing strategy, we were able to recover 87.2%, 98.8%, and 98.3% of the S, M, and L segments, respectively.

OROV whole-genome consensus sequences and genotyping. The 383 complete OROV consensus sequences of S, M, and L genomic segments generated in this study (382 from the current outbreak plus one from Tefé-AM 2015) were aligned with corresponding segments of all published full-length OROV genome sequences available at the NCBI (n = 72), sampled in the Americas between 1955 and 2021, including the prototype sequences of OROV ($OROV_P$ L: AF484424; M: AF441119; S: AY237111), Iquitos virus ($IQTV_P$ L: KF697142; M: KF697143; S: KF697144), Perdoes virus ($PEDV_P$ L: KP691627; M: KP691628; S: KP691629), and Madre de Dios virus ($MDDV_P$ L: KF697147; M: KF697145; S: KF697146). All these viruses are classified in the species *Orthobunyavirus oropoucheense*, having the classical OROV as the exemplar isolate of the species (https://ictv.global/report/chapter/peribunyaviridae/peribunyaviridae/orthobunyavirus). The resulting datasets were used to infer Bayesian phylogenetic trees for each genomic segment.

Bayesian phylogenetic trees were reconstructed under the best-fitted substitution model selected by jModelTest 2.1.10[94], using the MrBayes 3.2.7a program [95]. Two chains were run for 20×10^6 generations for each genomic segment, and the attainment of the stationary phase and the effective mixing of continuous parameters (effective sample size [ESS] > 200) were assessed using Tracer v1.7[96]. The consensus trees were visualized using the Treeio v3.1.7[97] and ggtree v3.2.1 R packages[98]. Clusters were defined by their statistical support (*posterior probability* [*PP*] > 0.90).

Bayesian evolutionary, phylogeographic, and demographic analyses. The temporal structure of the selected sequences was assessed using the program TempEst v.1.5.3[99] by a root-to-tip linear regression, in which the significance of the correlation between the collection date and genetic distance was accessed with a Spearman correlation test. Time-scaled phylogenetic trees for separate or concatenated genomic segments were estimated using the Bayesian Markov chain Monte Carlo (MCMC) approach, implemented in the software BEAST 1.10[100] with BEAGLE library v.3[101], to improve computational time. Bayesian trees were reconstructed using the GTR+G4+I nucleotide substitution model, the non-parametric Bayesian skyline coalescent demographic model,[102] and a relaxed molecular clock model with a continuous-time Markov chain (CTMC) rate reference prior.[103] We also explicitly modeled the OROV reassortment process in a Bayesian framework by applying the Coalescent With Reassortment Constant Population (CoalRe) model as available in the BEAST2 package.[45] An exponential distribution with a mean of 0.25 was set as the prior on the reassortment rate parameter. The analysis parameterization was complemented with the GTR+G4+I substitution model and a relaxed clock with a lognormal distribution model with default priors. As explained above, the spatial dispersion pattern of OROV in the Amazon region was reconstructed using both discrete and continuous phylogeographic analyses implemented in BEAST v.1.10.4.[100] For the discrete phylogeographic analysis, we employed a reversible discrete phylogeographic model[104] with a continuous-time Markov chain (CTMC) rate reference prior.[103] OROV sequences from AC, RO, and RR were grouped by state. In contrast, sequences from the state of AM were grouped by sub-state regions (AM-Central, AM-Southern, AM-Northern and AM-Southwestern), with the only exception of sequences from the capital city, Manaus, which belongs to the AM-Central region, but were grouped in a separate location due to the significant contribution of this city to the overall number of OROV cases and sequences. For the continuous phylogeographic reconstruction, we employed the Cauchy relaxed random walk model.[105] For the continuous phylogeographic analyses, a maximum of 10 genomes

per municipality (the earliest ones) were chosen to reduce the impact of within-municipality transmissions on the estimation of viral diffusion rates among Amazon municipalities. We assigned latitude and longitude coordinates to each sequence according to the municipality of origin. We selected the option *Add random jitter to tips*, adding noise to sampling coordinates to ensure unique geographic coordinates for each sequence. Multiple independent Markov chain Monte Carlo (MCMC) runs were performed and later combined to ensure that all continuous parameters had an effective sample size (ESS) > 200, as visualized in Tracer v1.7.[96] The maximum clade credibility (MCC) trees were summarized with TreeAnnotator v.1.10 and visualized using FigTree v.1.4.4 (http://tree.bio.ed.ac.uk/software/figtree/). Reassortment networks were visualized and edited in IcyTree.[106] Viral spatiotemporal diffusion was analyzed and visualized in SPREAD v.1.0.7[107] and further projected in maps generated with the ggplot2,[108] sf,[109] and geobr[110] R packages.

Statistical analyses. The Fisher exact test (two-tailed) was used to compare the frequency of symptoms between males and females infected with OROV. The threshold for statistical significance was set to $P < 0.05$ using two-sided tests. Statistical analyses were performed using GraphPad v.9.0 (Prism Software).

Data availability

All the OROV genomes generated and analyzed in this study were deposited at GenBank under accession numbers PP153945 to PP154172 and PQ064571 to PQ065491.

Acknowledgments

The authors wish to thank all the healthcare workers from the Brazilian States fighting the current Oropouche outbreak. We also appreciate the support of FIOCRUZ COVID-19 Genomics Surveillance Network members, the General Laboratory Coordination (CGLab) of the Brazilian Ministry of Health (MoH), Brazilian Central Laboratory States (LACENs) and health surveillance agencies from Acre, Amazonas, Rondônia, and Roraima. Funding support FAPEAM Call 04/2022/FIOCRUZ/FAPEAM/FAPERO - INOVAÇÃO NA AMAZÔNIA; Amazônia +10; FAPEAM Call 023/2022 - INICIATIVA AMAZÔNIA +10; Inova Fiocruz - Inova Amazônia; Rede Genômica de Vigilância em Saúde do Estado do Amazonas – REGESAM (Resolução nº. 002/2008, 007/2018 e 005/2019 – PRÓ-ESTADO/FAPEAM); Conselho Nacional de Desenvolvimento Científico e Tecnológico - CNPq Institutos Nacionais de Ciência e Tecnologia (INCT - VER) e Chamada CNPq/MCTI 10/2023 - Faixa B - Grupos Consolidados - Universal 2023 (421620/2023-4). GLW and GB are supported by the Conselho Nacional de Desenvolvimento Científico e Tecnológico (CNPq) through their productivity research fellowships (307209/2023-7 and 304883/2020-4). ED and AR are supported by Fundação de Amparo à Pesquisa e Inovação do Espírito Santo (FAPES).

Bibliography

1. Da Rosa, J. F. T. *et al.* Oropouche Virus: Clinical, Epidemiological, and Molecular Aspects of a Neglected Orthobunyavirus. *Am J Trop Med Hyg* 16–0672 (2017) doi:10.4269/ajtmh.16-0672.
2. Pereira-Silva, J. W. *et al.* Distribution and diversity of mosquitoes and Oropouche-like virus infection rates in an Amazonian rural settlement. *PLoS ONE* **16**, e0246932 (2021).
3. Cardoso, B. F. *et al.* Detection of Oropouche virus segment S in patients and in Culex quinquefasciatus in the state of Mato Grosso, Brazil. *Mem Inst Oswaldo Cruz* **110**, 745–754 (2015).
4. Pinheiro, F. P., Travassos Da Rosa, A. P. A., Gomes, M. L. C., LeDuc, J. W. & Hoch, A. L. Transmission of Oropouche Virus from Man to Hamster by the Midge *Culicoides paraensis*. *Science* **215**, 1251–1253 (1982).
5. Roberts, D. R., Hoch, A. L., Dixon, K. E. & Llewellyn, C. H. Oropouche virus. III. Entomological observations from three epidemics in Pará, Brazil, 1975. *Am J Trop Med Hyg* **30**, 165–171 (1981).
6. Wesselmann, K. M. *et al.* Emergence of Oropouche fever in Latin America: a narrative review. *The Lancet Infectious Diseases* S1473309923007405 (2024) doi:10.1016/S1473-3099(23)00740-5.
7. Figueiredo, L. T. M. Emergent arboviruses in Brazil. *Rev Soc Bras Med Trop* **40**, 224–229 (2007).
8. Sakkas, H., Bozidis, P., Franks, A. & Papadopoulou, C. Oropouche Fever: A Review. *Viruses* **10**, 175 (2018).
9. Mourão, M. P. G. *et al.* Oropouche Fever Outbreak, Manaus, Brazil, 2007–2008. *Emerg. Infect. Dis.* **15**, 2063–2064 (2009).
10. Tilston-Lunel, N. L. *et al.* Genetic analysis of members of the species Oropouche virus and identification of a novel M segment sequence. *Journal of General Virology* **96**, 1636–1650 (2015).
11. Carvalho, V. L. *et al.* Arbovirus outbreak in a rural region of the Brazilian Amazon. *Journal of Clinical Virology* **150–151**, 105155 (2022).
12. Vasconcelos, H. B. *et al.* Oropouche fever epidemic in Northern Brazil: Epidemiology and molecular characterization of isolates. *Journal of Clinical Virology* **44**, 129–133 (2009).
13. Azevedo, R. D. S. D. S. *et al.* Reemergence of Oropouche Fever, Northern Brazil. *Emerg. Infect. Dis.* **13**, 912–915 (2007).
14. Naveca, F. G., Nascimento, V. A., Souza, V. C. & Figueiredo, R. M. P. D. Human Orthobunyavirus Infections, Tefé, Amazonas, Brazil. *PLoS Curr* (2018) doi:10.1371/currents.outbreaks.7d65e5eb6ef75664da68905c5582f7f7.
15. Bastos, M. S. *et al.* Detection of *Herpesvirus* , *Enterovirus* , and *Arbovirus* infection in patients with suspected central nervous system viral infection in the Western Brazilian Amazon: Viral Infection in CNS, Amazon, Brazil. *J. Med. Virol.* **86**, 1522–1527 (2014).
16. Sciancalepore, S., Schneider, M. C., Kim, J., Galan, D. I. & Riviere-Cinnamond, A. Presence and Multi-Species Spatial Distribution of Oropouche Virus in Brazil within the One Health Framework. *TropicalMed* **7**, 111 (2022).
17. Fonseca, L. M. D. S., Carvalho, R. H., Bandeira, A. C., Sardi, S. I. & Campos, G. S. Oropouche Virus Detection in Febrile Patients' Saliva and Urine Samples in Salvador, Bahia, Brazil. *Jpn J Infect Dis* **73**, 164–165 (2020).
18. De Souza Costa, M. C. *et al.* Arbovirus investigation in patients from Mato Grosso during Zika and Chikungunya virus introdution in Brazil, 2015–2016. *Acta Tropica* **190**, 395–402 (2019).
19. Pinto De Figueiredo, R. M. *et al.* Identification of Oropouche Orthobunyavirus in the Cerebrospinal Fluid of Three Patients in the Amazonas, Brazil. *The American Journal of Tropical Medicine and Hygiene* **86**, 732–735 (2012).
20. Terzian, A. C. B. *et al.* Sporadic Oropouche Infection, Acre, Brazil. *Emerg. Infect. Dis.* **15**, 348–350 (2009).
21. De Thoisy, B., Gräf, T., Mansur, D. S., Delfraro, A. & Dos Santos, C. N. D. The Risk of Virus Emergence in South America: A Subtle Balance Between Increasingly Favorable Conditions and a Protective Environment. *Annual Review of Virology* (2024) doi:10.1146/annurev-virology-100422-024648.
22. Naveca, F. G. *et al.* Multiplexed reverse transcription real-time polymerase chain reaction for simultaneous detection of Mayaro, Oropouche, and Oropouche-like viruses. *Mem Inst Oswaldo Cruz* **112**, 510–513 (2017).
23. Sah, R. *et al.* Oropouche fever outbreak in Brazil: an emerging concern in Latin America. *The Lancet Microbe* S2666524724001368 (2024) doi:10.1016/S2666-5247(24)00136-8.
24. *Monitoramento Das Arboviroses e Balanço de Encerramento Do Comitê de Operações de Emergência (COE)*

Dengue e Outras Arboviroses 2024. vol. 55 https://www.gov.br/saude/pt-br/centrais-de-conteudo/publicacoes/boletins/epidemiologicos/edicoes/2024/boletim-epidemiologico-volume-55-no-11.pdf/view (2024).

25. Pinheiro, F. P., Travassos da Rosa, A. P., Travassos da Rosa, J. F. & Bensabath, G. An outbreak of Oropouche virus disease in the vicinity of Santarém, Pará, Brazil. *Tropenmed Parasitol* **27**, 213–223 (1976).
26. Purse, B. V., Carpenter, S., Venter, G. J., Bellis, G. & Mullens, B. A. Bionomics of Temperate and Tropical *Culicoides* Midges: Knowledge Gaps and Consequences for Transmission of *Culicoides* -Borne Viruses. *Annu. Rev. Entomol.* **60**, 373–392 (2015).
27. Veggiani Aybar, C. A., Dantur Juri, M. J., Lizarralde De Grosso, M. S. & Spinelli, G. R. Species diversity and seasonal abundance of *Culicoides* biting midges in northwestern Argentina. *Medical and Veterinary Entomology* **24**, 95–98 (2010).
28. Hoch, A. L., Roberts, D. R. & Pinheiro, F. P. Host-seeking behavior and seasonal abundance of Culicoides paraensis (Diptera: Ceratopogonidae) in Brazil. *J Am Mosq Control Assoc* **6**, 110–114 (1990).
29. Pinheiro, F. P., Pinheiro, M., Bensabath, G., Causey, O. R. & Shope, R. E. Epidemia de virus Oropouche em Belém. *Revista do Serviço de Saúde Pública (Rio de Janeiro)* **12**, 15–23 (1962).
30. Ciuoderis, K. A. *et al.* Oropouche virus as an emerging cause of acute febrile illness in Colombia. *Emerging Microbes & Infections* **11**, 2645–2657 (2022).
31. Gaillet, M. *et al.* Outbreak of Oropouche Virus in French Guiana. *Emerg Infect Dis* **27**, 2711–2714 (2021).
32. Durango-Chavez, H. V. *et al.* Oropouche virus infection in patients with acute febrile syndrome: Is a predictive model based solely on signs and symptoms useful? *PLoS ONE* **17**, e0270294 (2022).
33. Silva-Caso, W. *et al.* First outbreak of Oropouche Fever reported in a non-endemic western region of the Peruvian Amazon: Molecular diagnosis and clinical characteristics. *International Journal of Infectious Diseases* **83**, 139–144 (2019).
34. Rosa, A. P. A. T. *et al.* Epidemia de febre do Oropouche em Serra Pelada, município de Curionópolis, Pará, 1994. *Rev. Soc. Bras. Med. Trop.* **29**, 537–541 (1996).
35. Vasconcelos, P. F. D. C. *et al.* Primeiro registro de epidemias causadas pelo vírus Oropouche nos Estados do Maranhão e Goiás, Brasil. *Rev. Inst. Med. trop. S. Paulo* **31**, 271–278 (1989).
36. Moreira, H. M. *et al.* Outbreak of Oropouche virus in frontier regions in western Amazon. *Microbiol Spectr* **12**, e01629-23 (2024).
37. Gutierrez, B. *et al.* Evolutionary Dynamics of Oropouche Virus in South America. *J Virol* **94**, e01127-19 (2020).
38. Matthijnssens, J. *et al.* Recommendations for the classification of group A rotaviruses using all 11 genomic RNA segments. *Arch Virol* **153**, 1621–1629 (2008).
39. Argimón, S. *et al.* Microreact: visualizing and sharing data for genomic epidemiology and phylogeography. *Microb Genom* **2**, e000093 (2016).
40. Ladner, J. T. *et al.* Genomic and phylogenetic characterization of viruses included in the Manzanilla and Oropouche species complexes of the genus Orthobunyavirus, family Bunyaviridae. *Journal of General Virology* **95**, 1055–1066 (2014).
41. Aguilar, P. V. *et al.* Iquitos Virus: A Novel Reassortant Orthobunyavirus Associated with Human Illness in Peru. *PLoS Negl Trop Dis* **5**, e1315 (2011).
42. Saeed, M. F. *et al.* Jatobal virus is a reassortant containing the small RNA of Oropouche virus. *Virus Research* **77**, 25–30 (2001).
43. Briese, T., Calisher, C. H. & Higgs, S. Viruses of the family Bunyaviridae: Are all available isolates reassortants? *Virology* **446**, 207–216 (2013).
44. Hulo, C. *et al.* ViralZone: a knowledge resource to understand virus diversity. *Nucleic Acids Res* **39**, D576-582 (2011).
45. Müller, N. F., Stolz, U., Dudas, G., Stadler, T. & Vaughan, T. G. Bayesian inference of reassortment networks reveals fitness benefits of reassortment in human influenza viruses. *Proc. Natl. Acad. Sci. U.S.A.* **117**, 17104–17111 (2020).
46. Stubbs, S. H. *et al.* Vesicular Stomatitis Virus Chimeras Expressing the Oropouche Virus Glycoproteins Elicit Protective Immune Responses in Mice. *mBio* **12**, e00463-21 (2021).
47. Adhikari, U. K., Tayebi, M. & Rahman, M. M. Immunoinformatics Approach for Epitope-Based Peptide Vaccine Design and Active Site Prediction against Polyprotein of Emerging Oropouche Virus. *Journal of Immunology Research* **2018**, 1–22 (2018).
48. Causey, O. R., Laemmert, H. W. & Kumm, H. W. Dispersion of Forest Mosquitoes in Brazil: Further Studies 1. *The American Journal of Tropical Medicine and Hygiene* **s1-30**, 301–312 (1950).

49. Brenner, R. J., Wargo, M. J., Stains, G. S. & Mulla, M.S. The dispersal of Culicoides mohave (Diptera: Ceratopogonidae) in the desert of Southern California. *Mosquito News* **44**, 343–350 (1984).
50. Lillie, T. H., Marquardt, W. C. & Jones, R. H. The flight range of *Culicoides variipennis* (Diptera: Ceratopogonidae).. *Can Entomol* **113**, 419–426 (1981).
51. Auguste, A. J. *et al.* Yellow Fever Virus Maintenance in Trinidad and Its Dispersal throughout the Americas. *J Virol* **84**, 9967–9977 (2010).
52. Ribeiro Prist, P. *et al.* Roads and forest edges facilitate yellow fever virus dispersion. *Journal of Applied Ecology* **59**, 4–17 (2022).
53. Delatorre, E. *et al.* Distinct YFV Lineages Co-circulated in the Central-Western and Southeastern Brazilian Regions From 2015 to 2018. *Front. Microbiol.* **10**, 1079 (2019).
54. Hill, S. C. *et al.* Genomic Surveillance of Yellow Fever Virus Epizootic in São Paulo, Brazil, 2016 – 2018. *PLoS Pathog* **16**, e1008699 (2020).
55. Ellwanger, J. H. *et al.* Beyond diversity loss and climate change: Impacts of Amazon deforestation on infectious diseases and public health. *An. Acad. Bras. Ciênc.* **92**, e20191375 (2020).
56. Gottdenker, N. L., Streicker, D. G., Faust, C. L. & Carroll, C. R. Anthropogenic Land Use Change and Infectious Diseases: A Review of the Evidence. *EcoHealth* **11**, 619–632 (2014).
57. Parrish, C. R. *et al.* Cross-Species Virus Transmission and the Emergence of New Epidemic Diseases. *Microbiol Mol Biol Rev* **72**, 457–470 (2008).
58. Mordecai, E. A. *et al.* Thermal biology of mosquito-borne disease. *Ecology Letters* **22**, 1690–1708 (2019).
59. Bartlow, A. W. *et al.* Forecasting Zoonotic Infectious Disease Response to Climate Change: Mosquito Vectors and a Changing Environment. *Veterinary Sciences* **6**, 40 (2019).
60. Mills, J. N., Gage, K. L. & Khan, A. S. Potential Influence of Climate Change on Vector-Borne and Zoonotic Diseases: A Review and Proposed Research Plan. *Environ Health Perspect* **118**, 1507–1514 (2010).
61. De Souza, W. M. & Weaver, S. C. Effects of climate change and human activities on vector-borne diseases. *Nat Rev Microbiol* **22**, 476–491 (2024).
62. Barichivich, J. *et al.* Recent intensification of Amazon flooding extremes driven by strengthened Walker circulation. *Sci. Adv.* **4**, eaat8785 (2018).
63. Espinoza, J.-C., Marengo, J. A., Schongart, J. & Jimenez, J. C. The new historical flood of 2021 in the Amazon River compared to major floods of the 21st century: Atmospheric features in the context of the intensification of floods. *Weather and Climate Extremes* **35**, 100406 (2022).
64. Marengo, J. A. & Espinoza, J. C. Extreme seasonal droughts and floods in Amazonia: causes, trends and impacts. *Intl Journal of Climatology* **36**, 1033–1050 (2016).
65. NOAA. Recent Triple-Dip La Niña Upends Current Understanding of ENSO. (2023).
66. Li, X., Hu, Z., McPhaden, M. J., Zhu, C. & Liu, Y. Triple-Dip La Niñas in 1998–2001 and 2020–2023: Impact of Mean State Changes. *JGR Atmospheres* **128**, e2023JD038843 (2023).
67. Espinoza, J.-C. *et al.* The new record of drought and warmth in the Amazon in 2023 related to regional and global climatic features. *Sci Rep* **14**, 8107 (2024).
68. Flores, B. M. *et al.* Critical transitions in the Amazon forest system. *Nature* **626**, 555–564 (2024).
69. Gibb, R. *et al.* The anthropogenic fingerprint on emerging infectious diseases. Preprint at https://doi.org/10.1101/2024.05.22.24307684 (2024).
70. Romero-Alvarez, D., Escobar, L. E., Auguste, A. J., Del Valle, S. Y. & Manore, C. A. Transmission risk of Oropouche fever across the Americas. *Infect Dis Poverty* **12**, 47 (2023).
71. Romero-Alvarez, D. & Escobar, L. E. Vegetation loss and the 2016 Oropouche fever outbreak in Peru. *Mem. Inst. Oswaldo Cruz* **112**, 292–298 (2017).
72. IPAM. Amazônia em Chamas 9: O Novo e Alarmante Patamar do Desmatamento na Amazônia. (2024).
73. Santos, B., Ferreira, R., Dias, M. Brandão, I., Amorim, L., Souza Junior, C. Dinâmica do desmatamento na região AMACRO com o sistema de alerta de desmatamento (SAD). in *Anais do XX Simpósio Brasileiro de Sensoriamento Remoto* (INPE, Florianópolis, 2023).
74. Assis, L., Ferreira, K., Vinhas, L., Maurano, L., Almeida, C., Carvalho, A., Rodrigues, J., Maciel, A., Camargo, C. TerraBrasilis: A Spatial Data Analytics Infrastructure for Large-Scale Thematic Mapping. ISPRS International Journal of Geo-Information. 8, 513, 2019.
75. Ferrante, L. & Fearnside, P. M. Brazil's political upset threatens Amazonia. *Science* **371**, 898–898 (2021).
76. Silva Junior, C. H. L. *et al.* The Brazilian Amazon deforestation rate in 2020 is the greatest of the decade. *Nat Ecol Evol* **5**, 144–145 (2020).
77. Vale, M. M. *et al.* The COVID-19 pandemic as an opportunity to weaken environmental protection in Brazil. *Biological Conservation* **255**, 108994 (2021).

78. Brito, B., Barreto, P., Brandão, A., Baima, S. & Gomes, P. H. Stimulus for land grabbing and deforestation in the Brazilian Amazon. *Environ. Res. Lett.* **14**, 064018 (2019).
79. Chaves, M. E. D. *et al.* AMACRO: the newer Amazonia deforestation hotspot and a potential setback for Brazilian agriculture. *Perspectives in Ecology and Conservation* **22**, 93–100 (2024).
80. Superintendência do Desenvolvimento da Amazônia (SUDAM). PROJETO PREVÊ A CRIAÇÃO DE UMA ZONA ESPECIAL DE DESENVOLVIMENTO SUSTENTÁVEL NA AMAZÔNIA. (2024).
81. Superintendência do Desenvolvimento da Amazônia (SUDAM). Zona de desenvolvimento sustentável dos Estados do Amazonas, Acre e Rondônia 2021-2027: documento referencial. (2021).
82. Carrero, G. C., Walker, R. T., Simmons, C. S. & Fearnside, P. M. Land grabbing in the Brazilian Amazon: Stealing public land with government approval. *Land Use Policy* **120**, 106133 (2022).
83. De Oliveira, G. *et al.* Smoke pollution's impacts in Amazonia. *Science* **369**, 634–635 (2020).
84. Andrade, M. B., Ferrante, L. & Fearnside, P. M. Brazil's Highway BR-319 demonstrates a crucial lack of environmental governance in Amazonia. *Envir. Conserv.* **48**, 161–164 (2021).
85. Ferrante, L., Gomes, M. & Fearnside, P. M. Amazonian indigenous peoples are threatened by Brazil's Highway BR-319. *Land Use Policy* **94**, 104548 (2020).
86. Mataveli, G. A. V., Chaves, M. E. D., Brunsell, N. A. & Aragão, L. E. O. C. The emergence of a new deforestation hotspot in Amazonia. *Perspectives in Ecology and Conservation* **19**, 33–36 (2021).
87. Plowright, R. K. *et al.* Pathways to zoonotic spillover. *Nat Rev Microbiol* **15**, 502–510 (2017).
88. Layan, M. *et al.* Impact and mitigation of sampling bias to determine viral spread: Evaluating discrete phylogeography through CTMC modeling and structured coalescent model approximations. *Virus Evolution* **9**, vead010 (2023).
89. Liu, P., Song, Y., Colijn, C. & MacPherson, A. The impact of sampling bias on viral phylogeographic reconstruction. *PLOS Glob Public Health* **2**, e0000577 (2022).
90. Kalkauskas, A. *et al.* Sampling bias and model choice in continuous phylogeography: Getting lost on a random walk. *PLoS Comput Biol* **17**, e1008561 (2021).
91. Lambin, E. F., Tran, A., Vanwambeke, S. O., Linard, C. & Soti, V. Pathogenic landscapes: Interactions between land, people, disease vectors, and their animal hosts. *Int J Health Geogr* **9**, 54 (2010).
92. Quick, J. *et al.* Multiplex PCR method for MinION and Illumina sequencing of Zika and other virus genomes directly from clinical samples. *Nat Protoc* **12**, 1261–1276 (2017).
93. Untergasser, A. *et al.* Primer3--new capabilities and interfaces. *Nucleic Acids Res* **40**, e115 (2012).
94. Darriba, D., Taboada, G. L., Doallo, R. & Posada, D. jModelTest 2: more models, new heuristics and parallel computing. *Nat Methods* **9**, 772–772 (2012).
95. Ronquist, F. *et al.* MrBayes 3.2: efficient Bayesian phylogenetic inference and model choice across a large model space. *Syst Biol* **61**, 539–542 (2012).
96. Rambaut, A., Drummond, A. J., Xie, D., Baele, G. & Suchard, M. A. Posterior Summarization in Bayesian Phylogenetics Using Tracer 1.7. *Syst Biol* **67**, 901–904 (2018).
97. Wang, L.-G. *et al.* Treeio: An R Package for Phylogenetic Tree Input and Output with Richly Annotated and Associated Data. *Molecular Biology and Evolution* **37**, 599–603 (2020).
98. Yu, G., Smith, D. K., Zhu, H., Guan, Y. & Lam, T. T. GGTREE : an R package for visualization and annotation of phylogenetic trees with their covariates and other associated data. *Methods Ecol Evol* **8**, 28–36 (2017).
99. Rambaut, A., Lam, T. T., Max Carvalho, L. & Pybus, O. G. Exploring the temporal structure of heterochronous sequences using TempEst (formerly Path-O-Gen). *Virus Evol* **2**, vew007 (2016).
100. Suchard, M. A. *et al.* Bayesian phylogenetic and phylodynamic data integration using BEAST 1.10. *Virus Evol* **4**, vey016 (2018).
101. Ayres, D. L. *et al.* BEAGLE 3: Improved Performance, Scaling, and Usability for a High-Performance Computing Library for Statistical Phylogenetics. *Systematic Biology* **68**, 1052–1061 (2019).
102. Drummond, A. J. Bayesian Coalescent Inference of Past Population Dynamics from Molecular Sequences. *Molecular Biology and Evolution* **22**, 1185–1192 (2005).
103. Ferreira, M. A. R. & Suchard, M. A. Bayesian analysis of elapsed times in continuous-time Markov chains. *Can J Statistics* **36**, 355–368 (2008).
104. Lemey, P., Rambaut, A., Drummond, A. J. & Suchard, M. A. Bayesian Phylogeography Finds Its Roots. *PLoS Comput Biol* **5**, e1000520 (2009).
105. Lemey, P., Rambaut, A., Welch, J. J. & Suchard, M. A. Phylogeography Takes a Relaxed Random Walk in Continuous Space and Time. *Molecular Biology and Evolution* **27**, 1877–1885 (2010).
106. Vaughan, T. G. IcyTree: rapid browser-based visualization for phylogenetic trees and networks. *Bioinformatics* **33**, 2392–2394 (2017).

107. Bielejec, F., Rambaut, A., Suchard, M. A. & Lemey, P. SPREAD: spatial phylogenetic reconstruction of evolutionary dynamics. *Bioinformatics* **27**, 2910–2912 (2011).
108. Wickham, H. *Ggplot2*. (Springer International Publishing, Cham, 2016). doi:10.1007/978-3-319-24277-4.
109. Pebesma, E. Simple Features for R: Standardized Support for Spatial Vector Data. *The R Journal* **10**, 439 (2018).
110. Pereira, R. H. M., Gonçalves, C. N. & al, et. geobr: Loads Shapefiles of Official Spatial Data Sets of Brazil. (2019).

Supplementary Table 1 - Signs and symptoms observed in Oropouche fever patients from Amazonas State, Brazil, 2024.

Signs/Symptoms	Female N = 1,085	Male N = 1,187	Two-tailed Fisher exact test
Fever	1,044 (96.8)	1,153 (97.5)	0.2408
Headache	1,012 (93.8)	1,084 (91.7)	0.0845
Myalgia	854 (79.1)	913 (77.2)	0.3127
Nausea	501 (46.4)	450 (38.1)	**> 0.0001**
Retro-orbital pain	367 (34)	403 (34.1)	0.9646
Arthralgia	313 (29)	332 (28.1)	0.6751
Vomiting	314 (29.1)	268 (22.7)	**0.0005**
Photophobia	101 (9.4)	89 (7.5)	0.1293
Diarrhea	89 (8.2)	79 (6.7)	0.1726
Rash	35 (3.2)	28 (2.4)	0.2496
Edema	35 (3.2)	28 (2.4)	0.2496
Other signs/symptoms	330 (30.6)	361 (30.5)	1.0000

In 2024, 2,272 Oropouche fever patients from the Amazonas State, 1,085 females, and 1,187 males, answered the medical form. The absolute number for each sign/symptom and the percentage (in brackets) related to the total number for each gender are shown. The Two-tailed Fisher exact test results are shown in the fourth column, and those statistically significant are highlighted in bold.

Supplementary Table 2. Primers designed and used to sequence near-to-complete Oropouche virus genomes in this study.

Name	Sequence	Sequence Length
OROV_L_v2_1_LEFT	ACAATCTCAAAATGTCGCAACTGTT	25
OROV_L_v2_1_RIGHT	TGAAGGATCCAACCTGATAATAACGA	26
OROV_L_v2_2_LEFT	CGGTCTTCCAGAATTACAAGAGAGAA	26
OROV_L_v2_2_RIGHT	CTGCTCCGAATGATTTGAATTCCAA	25
OROV_L_v2_3_LEFT	ACTCCAGAATTGCTTACTCATCCT	24
OROV_L_v2_3_LEFT_alt	ACTCCAGAATTGCTTGCTCATCCT	24
OROV_L_v2_3_RIGHT	CCACTCATGGCTTGCAATGATTT	23
OROV_L_v2_4_LEFT	ACCAAGCATACATTTTATATGGGCAC	26
OROV_L_v2_4_RIGHT	AGGCTTATCGGTATTTATGTCATTGTTTAG	30
OROV_L_v2_5_LEFT	ACGGATGTCATAAAAAGAGAAGACAGA	27
OROV_L_v2_5_RIGHT	TTTGCACATGAGACAATCCTAAAGG	25
OROV_L_v2_6_LEFT	CCAAGTACTGGCAATGCATCAAC	23
OROV_L_v2_6_RIGHT	GAAAAGCCTAGTAACTTATCAAACTCTAGAC	31
OROV_L_v2_7_LEFT	AGAAAGGTGTCAGCGCATAGTG	22
OROV_L_v2_7_RIGHT	GAACCAAATGGATTTAAGATCTCTTTTGG	29
OROV_L_v2_8_LEFT	CAGAGGAAAAAGGTCCAAATAAGGG	25
OROV_L_v2_8_LEFT_alt	CAGAGGAAAAAGGTCCAAATAAGGG	25
OROV_L_v2_8_RIGHT	AAGGTGGATATTGTTGTTATAGACCTGT	28
OROV_L_v2_9_LEFT	GCAAGGAATTTGAACTTAGATACTTCAAGA	30
OROV_L_v2_9_RIGHT	TGCTTCTTCATAGTCTCTAAAATCAACTTG	30
OROV_L_v2_10_LEFT	TGTCCGTAAAAGTTTTTGACAGACT	25
OROV_L_v2_10_LEFT_alt	TGTCTGTAAAAGTTTTTGATAGACT	25
OROV_L_v2_10_LEFT_alt1	TGTCTGTAAAAGTTTTTGATAGATT	25
OROV_L_v2_10_RIGHT	CCCTCGTGCCTTACTTTCACAT	22
OROV_L_v2_10_RIGHT_alt	CCCTCGTGCCTTACTTTCACAT	22
OROV_L_v2_10_RIGHT_alt1	CCCTCGTGCTTTACTTTCACAT	22
OROV_L_v2_11_LEFT	TCAGCAACACAATAAAGACATTGGG	25
OROV_L_v2_11_RIGHT	ACTACAGCTGTGCAAGTAACTACT	24
OROV_L_v2_12_LEFT	GGGTTGATGACAAACAATTATAGATCCAA	29
OROV_L_v2_12_LEFT_alt	GGGGTGATGACAAACAATTATAGATCCAA	29
OROV_L_v2_12_RIGHT	GCAGTAAGCAAAAACCTCCCGT	22
OROV_L_v2_13_LEFT	GGAAATCAGGCAAACATGAAAAAGAC	26
OROV_L_v2_13_RIGHT	GTGACATTTCCCGCTTCTAAACC	23
OROV_L_v2_14_LEFT	AAATACCAGTGGAGATGTGCGG	22
OROV_L_v2_14_RIGHT	GCTCGTTTGTCTTATCCTCATCTGT	25
OROV_L_v2_15_LEFT	TTAACACCTCGTAAATTCACAACGA	25
OROV_L_v2_15_RIGHT	AAGTTGCTTAAATCATCTACAATCTGGAC	29
OROV_L_v2_16_LEFT	AGCATACATGATAAGATTTTTGGATTGCA	29

OROV_L_v2_16_RIGHT	TGTGCTTTGTATGAAATCTTCCAGATG	27
OROV_L_v2_17_LEFT	TGTGAGAGGGCCAACAAATGTG	22
OROV L v2 17 RIGHT	TCCAATTCAGGTGAGGACGAGA	22
OROV L v2 18 LEFT	GCGCACTGACAGGGAACTTAAT	22
OROV L v2 18 RIGHT	TGGTCCGGTGTTCATGTCTCT	21
OROV_L_v2_18_RIGHT_alt	TGGTCCAGTGTTCATATCTCT	21
OROV_L_v2_19_LEFT	TTGGACAAGTTTGATGCAGATAAATCA	27
OROV_L_v2_19_RIGHT	AGGAACCCATTTTGAATCTCTGTTTAAC	28
OROV_L_v2_19_RIGHT_alt	AGGAACCCATTTTGAATCTCTGTTTAAC	28
OROV L v2 20 LEFT	GGTACTTCTATTCTATATTGCCCACCC	27
OROV L v2 20 LEFT alt	GGTACTTCTATTCTATATTGCCCACCC	27
OROV L v2 20 RIGHT	TTGGTCATTTTCACTGCCATTGC	23
OROV L v2 21 LEFT	TCTATCAGAGTTAATGAAATCCACATCCT	29
OROV L v2 21 RIGHT	TTGTCTAGTTCTGTGGACCACTG	23
OROV L v2 22 LEFT	GCATTCGACTTTCTTGACATGGG	23
OROV_L_v2_22_RIGHT	TGGATTTCCCAGTTTTCTTACTTTTGT	27
OROV_M_400_1_LEFT	GCAACAAACAGTGACAATGGCG	22
OROV_M_400_1_LEFT_alt1	ACCAGCAACAAACAGTGACA	20
OROV_M_400_1_RIGHT	GCTGCTCTACATGTGTACATTTTAGG	26
OROV_M_400_2_LEFT	TCTGAGTGCAATCCAGTGCTAGA	23
OROV M 400 2 LEFT alt1	TCTGAATGCAATCCAGTGTTAGA	23
OROV M 400 2 LEFT alt2	TCTGAATGTAATCCAGTGCTAGA	23
OROV M 400 2 RIGHT	ACATTGCTTCAATCATTGAGTATGGC	26
OROV_M_400_3_LEFT	TGTGGTCAGAAATCAATAAAATTCCATGC	29
OROV_M_400_3_RIGHT	GCACCTTAAGAGCTTCTGTGCA	22
OROV_M_400_4_LEFT	CCTGCCCAAATTGTCTACTTGCA	23
OROV_M_400_4_RIGHT	AAATGCTGAAAAGCCGGTTGAAT	23
OROV_M_400_4_RIGHT_alt1	AAATGTTGAAAAGCCGGTTGAAT	23
OROV_M_400_5_LEFT	AGAAATGGAAGTCTTGAAGCAGTCA	25
OROV_M_400_5_RIGHT	CAAGCAATCTTCATCTGCATAAACTGT	27
OROV_M_400_6_LEFT	TGCAAATTTAGTCCAAGAGTAAACCACT	28
OROV_M_400_6_RIGHT	GCGCCAGGCAACATTATAAGGT	22
OROV M 400 7 LEFT	AGTTTGCCCAAGATTCACATAGAATGA	27
OROV_M_400_7_RIGHT	GCCTTAAGAGCATCAGAGTCATCT	24
OROV_M_400_8_LEFT	GCTGACCTGAACACCATAATGGA	23
OROV_M_400_8_LEFT_alt1	GCTGACCTGAATACCATAATGGA	23
OROV_M_400_8_RIGHT	AAAGCAGGTGGTTTGTATGCGG	22
OROV_M_400_8_RIGHT_alt1	AAAGCAGGTGATTTGTGTGCGG	22
OROV_M_400_8_RIGHT_alt2	AAAGTAGGTGATTTGTGTGCGG	22
OROV M 400 9 LEFT	ACGAAATTCCCAAATCTAATCCTTTTACTG	30
OROV M 400 9 RIGHT	CCACAGAATACGATCGGCCATG	22
OROV M 400 10 LEFT	CGCAACCAGCAGATATGCAGAC	22

OROV_M_400_10_RIGHT	GTGGAAGGTTCTTTGTGGGCTT	22
OROV_M_400_11_LEFT	AGACCCACAAAGAATTTAGCACTATGA	27
OROV M 400 11 RIGHT	CAGGAATCTTTTCGGGGCAGTG	22
OROV M 400 12 LEFT	AGCACAGTACCAGAAAGCATACAC	24
OROV M 400 12 RIGHT	AGGGTCGGAAGTTGGTTAGTCT	22
OROV M 400 13 LEFT	ACTTTGCCTCATGAAACTTATTGCAA	26
OROV_M_400_13_RIGHT	TTTGGCCCATGTTTGATCCTGT	22
OROV_M_400_14_LEFT	TGACAATTATCAGTCATGCACTAGGTT	27
OROV_M_400_14_RIGHT	ATGTCTCTCCCACAGATATGTGCT	24
OROV M 400 15 LEFT	CTGCCATTGTAAAACAAACTGTGAAGA	27
OROV M 400 15 RIGHT	CCGACCTATGGGCAACAGGATAT	23
OROV M 400 16 LEFT	ACAATCAGAAGATAGATTTGTCGCAGTT	28
OROV M 400 16 RIGHT	TGTGCTACCAACAACAATTTTTGACT	26
OROV S 400 1 LEFT	TCCAATAATGTCAGAGTTCATTTTCAATGA	30
OROV S 400 1 RIGHT	GCCCTAAACTCAGCTTGCTTAATTGG	26
OROV_S_400_2_LEFT	CAGTTCCAGTCGAATCCAGTGC	22
OROV_S_400_2_RIGHT	TCTCTTGCTGCTGGGGAGAATC	22
OROV_S_400_3_LEFT	CGGCATGGATGTCAACTTTATGAAG	25
OROV_S_400_3_RIGHT	TGACATAGCTTTCCCCAACCAC	22

Using these primers, we were able to sequence 87.2%, 98.8%, and 98.3% of the S, M, and L segments, respectively.